

The Cryosphere Discuss., author comment AC6  
<https://doi.org/10.5194/tc-2021-163-AC6>, 2021  
© Author(s) 2021. This work is distributed under  
the Creative Commons Attribution 4.0 License.



## **Comment on tc-2021-163**

Alain Royer et al.

---

Author comment on "Review article: Performance assessment of radiation-based field sensors for monitoring the water equivalent of snow cover (SWE)" by Alain Royer et al., The Cryosphere Discuss., <https://doi.org/10.5194/tc-2021-163-AC6>, 2021

---

Revised paper with track change

Please also note the supplement to this comment:

<https://tc.copernicus.org/preprints/tc-2021-163/tc-2021-163-AC6-supplement.pdf>

1  
2  
3 **Review article: Performance assessment of radiation-based field sensors**  
4 **for monitoring the water equivalent of snow cover (SWE)**  
5  
6

7 Alain Royer<sup>a,b\*</sup>, Alexandre Roy<sup>b,c</sup>, Sylvain Jutras<sup>d</sup>, Alexandre Langlois<sup>a,b</sup>

8  
9 <sup>a</sup>Centre d'Applications et de Recherche en Télédétection (CARTEL), Université de Sherbrooke, Sherbrooke,  
10 Québec, Canada

11 <sup>b</sup>Centre d'études nordiques (CEN), Québec, Canada

12 <sup>c</sup>Département des Sciences de l'Environnement, Université du Québec à Trois-Rivières, Trois-Rivières,  
13 Québec, Canada

14 <sup>d</sup>Département des sciences du bois et de la forêt, Université Laval, Québec City, Québec, Canada

15 \* Corresponding author  
16

17 **Abstract**

18 Continuous and spatially distributed data of snow mass (water equivalent of snow  
19 cover, SWE) from automatic ground-based measurements are increasingly required for  
20 climate change studies and for hydrological applications (snow hydrological model  
21 improvement and data assimilation). We present and compare four new-generation  
22 sensors, now commercialized, that are non-invasive based on different radiations that  
23 interact with snowpack for SWE monitoring: Cosmic Ray Neutron Probe (CRNP); Gamma  
24 Ray Monitoring (GMON) scintillator; frequency-modulated continuous-wave radar  
25 (FMCW-Radar) at 24 GHz; and Global Navigation Satellite System (GNSS) receivers  
26 (GNSSr). All four techniques have relatively low power requirements, provide  
27 continuous and autonomous SWE measurements, and can be easily installed in remote  
28 areas. A performance assessment of their advantages, drawbacks and uncertainties are  
29 discussed from experimental comparisons and a literature review. Relative uncertainties  
30 are estimated to range between 9 and 15% when compared to manual in situ snow  
31 surveys that are also discussed. Results show: • CRNP can be operated in two modes of  
32 functioning: beneath the snow, it is the only system able to measure very deep  
33 snowpacks (> 2000 mm w.e.) with reasonable uncertainty across a wide range of  
34 measurements; CRNP placed above the snow allows SWE measurements over a large  
35 footprint (~20 ha) above a shallow snowpack; in both cases, CRNP needs ancillary  
36 atmospheric measurements for SWE retrieval. • GMON is the most mature instrument  
37 for snowpacks that are typically up to 800 mm w.e.; Both instruments, CRNP (above  
38 snow) and GMON, are sensitive to surface soil moisture. • FMCW-Radar needs auxiliary  
39 snow depth measurements for SWE retrieval and is not recommended for automatic  
40 SWE monitoring (limited to dry snow). FMCW-radar is very sensitive to wet snow,  
41 making it a very useful sensor for melt detection (e.g., wet avalanche forecasts); • GNSSr  
42 allows three key snowpack parameters to be estimated simultaneously: SWE (range: 0 -  
43 1000 mm w.e.), snow depth and liquid water content, according to the retrieval

44 [algorithm that is used. Its low cost, compactness and low mass suggest a strong](#)  
45 [potential for GNSSr application in remote areas.](#)

46 **Key word:** ~~Snow Water Equivalent~~, electromagnetic wave sensors, Cosmic Ray Neutron  
47 Probe, Gamma Ray Monitoring, frequency-modulated continuous-wave radar, Global  
48 Navigation Satellite System, sensor performance review

## 49 50 **1. Introduction**

51 Snow cover on the ground [surface](#) plays an important role in the climate system due to  
52 its high albedo, heat insulation that affects the ground thermal regime, and its  
53 contribution to snow runoff and soil moisture. ~~Snow water equivalent~~ (SWE, its mass  
54 per unit area) [is expressed in kg m<sup>-2</sup>, but also is commonly shown in units of mm of](#)  
55 [water equivalent, mm w.e.](#) It is an Essential Climate Variable (ECV) for monitoring  
56 climate change, as recognized by the Global Climate Observing System (GCOS-~~WMO~~,  
57 [2016; https://gcos.wmo.int/en/essential-climate-variables.](https://gcos.wmo.int/en/essential-climate-variables)), [which aligns](#) with the  
58 WMO-Global Cryosphere Watch Initiative (Key et al., 2016;  
59 <https://globalcryospherewatch.org>). SWE monitoring is also of primary importance for  
60 hydrological forecasting and preventing flooding risks over snowmelt-dominated basins  
61 in mountainous and cold climate regions. [Snow station distributions are](#) generally sparse  
62 in high latitude regions, remote areas and high mountains (Bormann et al., 2013; Key et  
63 al., [2015, 2016](#); Pirazzini et al., 2018; [Heberkorn, 2019](#); Brown et al., 2019, 2021; Royer  
64 et al., 2021), given that monitoring is generally based upon expensive and occasional  
65 (weekly to monthly) manual sampling. [Automation of SWE measurement](#) networks is an  
66 essential medium-term prospect, especially since reliable and automatic instrument  
67 alternatives exist (Dong, 2018; [this study](#)).

68  
69 Various in situ field devices and approaches for measuring the temporal dynamics of  
70 SWE are available, all of which have their strengths and limitations (see the review by  
71 Rasmussen et al., 2012; Kinar and Pomeroy, 2015; Pirazzini et al., 2018). Some are  
72 invasive (i.e., destroying the snowpack or changing its properties), while others that are  
73 based on different remotely sensed approaches are non-invasive. Here, we focus on a  
74 new generation of [radiation](#)-based field sensors that directly measure SWE, i.e.,  
75 measuring a signal that is proportional to the snow mass per unit area. In this study, we  
76 do not consider [sensors that are based on pressure and load cell sensors \(snow](#)  
77 [pillows\), snowmelt lysimeters, dielectric sensors \(e.g., the SNOWPOWER system,](#)  
78 [commercially available as the Snowpack Analyzer\) or acoustic sensors \(see Kinar and](#)  
79 [Pomeroy, 2015\).](#) [Neither do we consider](#) indirect approaches, such as those based on  
80 snow-depth monitoring, combined with a model of snow density evolution (Yao et al.,  
81 2018). We also [exclude](#) satellite-based approaches.

82  
83 The objective of this paper, therefore, is to present a performance review of four  
84 selected non-invasive sensors (Table 1), viz., the Cosmic Ray Neutron Probe (CRNP), the  
85 Gamma Ray Monitoring (GMON) scintillator, frequency-modulated continuous-wave  
86 radar (FMCW-Radar) and Global Navigation Satellite System (GNSS) receivers ([GNSSr](#)).

87 All four approaches have common features: easy to install; low power (e.g., powered by  
88 solar panels); provide continuous and autonomous SWE measurements; and deployable  
89 in remote areas. The continuous or quasi-continuous SWE measurement capability is  
90 defined here relative to the application, such as for seasonal SWE monitoring, for  
91 hydrological model validation, or to follow an event of a short winter storm. Surface-  
92 based radar scatterometers and microwave radiometers have not been considered in  
93 this study because 1) they are still in early stages of development or are currently not  
94 operational, and 2) they have heavy maintenance demands (not autonomous) and are  
95 still relatively expensive. These include, for example, scatterometers (Werner et al.,  
96 2010; Wiesmann et al., 2010; King et al., 2015; Werner et al., 2019), microwave  
97 radiometers (Langlois, 2015; Roy et al., 2016, 2017; Wiesmann et al., 2021); radar  
98 interferometers (Werner et al., 2010; Leinss et al., 2015; Pieraccini and Miccinesi, 2019;  
99 GPRI brochure, 2021), and Stepped-Frequency Continuous Wave Radar (SFCW)  
100 instruments (Alonso et al., 2021).

101  
102 Sect. 2 provides background information on the basic principles of each of the four  
103 sensors that are presented in Table 1. Examples of SWE temporal series comparisons  
104 from four different instruments that were acquired in Québec, Eastern Canada, are  
105 given in Sect. 3.1 and 3.2: comparisons between EDF's CRNP (NRC sensor) and GMON on  
106 one hand, and GNSSr, FMCW-Radar and GMON on the other hand. This permits  
107 performance evaluations for each system, including uncertainty analysis, compared to  
108 manual SWE measurements. We complement these uncertainty assessments with a  
109 review of additional results from previous studies (Sect. 3.3, Table 2). Advantages and  
110 drawbacks of these sensors are then discussed in Sect. 4 (Table 3).

## 111 112 **2. Radiation-based SWE sensor review**

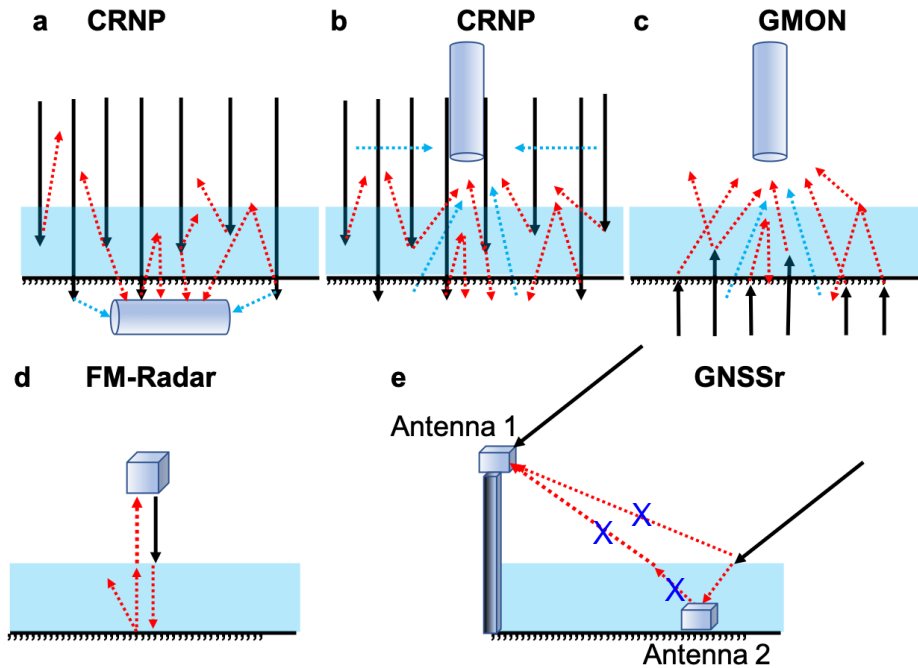
113 The main characteristics of the four reviewed sensors are summarized in Table 1, with  
114 the acronym that is used to denote them, together with their commercial names. There  
115 are two operation modes for the Cosmic Ray Neutron Probe (CRNP); thus, five cases  
116 were considered. All of these sensors allow quasi-continuous measurements throughout  
117 the winter without maintenance, and are powered by solar panels and batteries. The  
118 measuring principles of each of the instruments are illustrated in Fig. 1 and shown in Fig.  
119 2. In this section, we only recall the main principles of functioning and the key elements  
120 of SWE retrieval, given that all sensors are well described in detail in the cited  
121 references.

122  
123 Aspects that are related to the measurement scale of each sensor are critical to SWE  
124 measurements, since SWE is generally highly variable spatially, depending upon the  
125 ecosystem and terrain (Kinar and Pomeroy, 2015; Dong, 2018). These questions are  
126 discussed in Sect. 4.

129 Table 1. SWE sensors that were studied and acronyms that were used. FMCW:  
 130 frequency-modulated continuous-wave radar; GNSS: Global Navigation Satellite System,  
 131 including GPS (USA), GLONASS (Russia), Galileo (Europe) and Beidou (China) satellite  
 132 constellations. The frequency (Freq.) of the electromagnetic (EM) wave that was used  
 133 and their approximate maximum ~~Snow Water Equivalent~~ (SWE<sub>max</sub>) measurement limit  
 134 capabilities are given. SD: snow depth. See Fig. 1 for measurement principle  
 135 conceptualization and Fig. 2 for photos.  
 136

Sensor	Acronym	Approach	Freq. GHz	SWE <sub>max</sub> (mm)	Comments	Commercial Name	Main recent references
Cosmic Ray Neutron Probe	CRNP	Sensor beneath snowpack	-	<u>up to</u> 2000	Measures total snow, ice and water amount	SnowFox	<a href="https://hydroinnova.com">https://hydroinnova.com</a>
		Sensor above snowpack		~ 150-300		Hydroinnova CRS-1000/B	<a href="https://hydroinnova.com">https://hydroinnova.com</a> Bogena et al., 2020
							NRC EDF-Fr
Gamma Ray scintillator	GMON	Sensor above snowpack	3.53 10 <sup>11</sup> 6.31 10 <sup>11</sup>	<u>up to</u> <u>600-</u> <u>800</u>	Measures total snow, ice and water amount	CS725 Campbell Sci.	Choquette et al., 2013 Smith et al., 2017 <a href="http://www.campbellsci.ca">http://www.campbellsci.ca</a>
Frequency-modulated continuous-wave Radar	FMCW-Radar	Active sensor above snowpack	24	~1000	Requires <u>SD</u> measurements Also measures stratigraphy	Sentire™ sR-1200 IMST Inc.	Pomerleau et al., 2020 <a href="https://shop.imst.de">https://shop.imst.de</a>
Global Navigation Satellite System receivers	GNSSr	2 antennas above/beneath snowpack	1.575 - 1.609	<u>Up to</u> 1500	Measures also Liquid Water Content <u>and SD estimates</u>	SnowSense	Henkel et al., 2019 Koch et al., 2020 <a href="https://www.vista-geo.de/en/snowsense/">https://www.vista-geo.de/en/snowsense/</a>

137  
 138  
 139



140  
 141  
 142  
 143  
 144  
 145  
 146  
 147  
 148  
 149  
 150  
 151  
 152  
 153  
 154  
 155  
 156

**Figure 1** Diagram of radiation paths for the five approaches (see Table 1). In all figures, black arrows correspond to natural (a, b, c) or emitted (d, e) signals and dotted red arrows to rays interacting with snow (the lower the signal reaching the sensor, the higher the SWE). **a)** Cosmic Ray Neutron Probe (CRNP) below the snow, buried in the ground. In this case, black arrows are ambient neutrons generated primarily by interactions of secondary cosmic ray neutrons with terrestrial and atmospheric nuclei. Dotted red arrows are neutrons interacting with snow, which decrease when SWE increases. Dotted blue arrows are neutrons interacting with soil moisture. **b)** CRNP above the snow, looking downward. Same as (a) for the arrow meanings, but dotted blue arrows are neutrons interacting with soil and atmospheric moisture. **c)** Gamma Ray Monitor (GMON) sensor. Same as (a) for the arrow meanings. **d)** Frequency-modulated continuous-wave radar (FMCW-Radar) looking downward above the snow. Black arrow is the radar-emitted wave at 24 GHz. **e)** Global Navigation Satellite System (GNSS) receivers. The two antennas receive signals emitted by all of the GNSS satellites in the antennas' field of view and at all incidence angles; only one incident ray (black arrow) at one angle is shown. According to the inversion algorithm, different rays that interact with the snow (dotted red arrows) are used. For the SnowSense system, independent measurements at antenna 1 and antenna 2 are analyzed.



157

158 Figure 2. Photographs of sensors that were analyzed. **a**) Cosmic Ray Neutron Probe (CRNP) from the EDF  
 159 French network (Nivomètre à Rayon Cosmic\_NRC) at the Lac noir station in Ecrins-Pelvoux massif, France.  
 160 One can see the neutron probe buried in the ground (also shown in inset) and the mast, which carries  
 161 ancillary meteorological sensors. Credit: Delunel et al. (2014). **b**) SnowFox CRNP set at ground level  
 162 beneath the snow cover. Similar to (a), the system requires measurements of atmospheric conditions.  
 163 Credit: Hydroinnova SnowFox manual. **c**) Same sensor as in (b), but the Hydroinnova CRS-1000/B sensor is  
 164 placed above the snow, measuring ambient and upward neutron counts, with the latter being attenuated  
 165 by the snowpack. Crédit: Philip Marsh, Wilfrid Laurier University, Waterloo, ON, Canada; sensor in the  
 166 tundra at Trail Valley Creek, Changing Cold Regions Network <http://ccrnetwork.ca>. **d**) GNSSr  
 167 installed at the Université de Sherbrooke SIRENE site. The antenna that was placed on the ground (beneath the snow)  
 168 was made visible at 3 m from the mast, on top of which a second antenna was affixed. Credits: Alain  
 169 Royer. **e**) The FMCW-Radar (on the left) and the GMON (on the right) at the NEIGE-Forêt Montmorency  
 170 site. A metallic plate on the ground in the field-of-view of the radar substantially increases radar echoes.  
 171 In the background of photo (e), one can see the solid precipitation gauge, which is known as the Double  
 172 Fence Intercomparison Reference (DFIR). Credits: Alain Royer. **f**) Meteorological and snow (GMON)  
 173 automatic station at the LeMoynes James-Bay, Québec, Canada site in a sub-arctic environment (Prince et  
 174 al., 2019). Credits: Alain Royer. **g**) The GMON at the NEIGE-Forêt Montmorency site set up to boost <sup>40</sup>K  
 175 counts with pipes filled with potassium fertilizer. Credit: Sylvain Jutras.

176 2.1 Cosmic Ray Neutron probe (CRNP)

177 CRNP measurement is based on the moderation of ambient neutrons by hydrogen in  
 178 water, snow and ice. The intensity of natural low-energy cosmic ray neutron emission is  
 179 inversely correlated with the amount of hydrogen in the soil (Zreda et al. 2008;  
 180 Andreasen et al., 2017) or snow cover (Desilets et al. 2010; Gottardi et al., 2013; Sigouin  
 181 and Si, 2016; Gugerli et al., 2019; Bogena et al., 2020). Even though the principle of this  
 182 approach has been known since the 1970s, it attained a level of operational maturity in  
 183 the 2000s, especially with the use of commercialized soil moisture probes. Électricité de

184 France (EDF) successfully used a network of cosmic-ray probes (denoted Nivomètre à  
185 Rayon Cosmique, NRC; this sensor is composed of two neutron detector tubes filled  
186 with Helium 3,  $^3\text{He}$ ) that were buried under the snowpack to measure SWE for more  
187 than a decade in the French Alps and in the Pyrenees (Fig. 2a, sensor placed at 3.5 m  
188 from a 6 m mast) (Paquet and Laval, 2006; Paquet et al., 2008; Gottardi et al., 2013;  
189 Delunel et al., 2014). Ephemeral, shallow snow cover across the UK is monitored by the  
190 COSMOS-UK network of 46 sites equipped with the CRNP Hydroinnova CRS-2000 or CRS-  
191 1000/B models (<https://cosmos.ceh.ac.uk>; Evans et al., 2016).

192  
193 There are two experimental approaches for CRNP-based SWE monitoring (Fig. 1a,b): 1)  
194 with the probe at the ground level beneath the snow (such as EDF' NRC, Fig. 2a, and the  
195 SnowFox sensor for Hydroinnova, Fig. 2b), or 2) with the probe placed a few meters  
196 above the snow surface (Fig. 1b), such as the one proposed by Hydroinnova (Fig. 2c)  
197 (CRS-1000/B, Hydroinnova, Albuquerque, NM, USA; [http://hydroinnova.com/](http://hydroinnova.com/snow_water.html)  
198 [snow\\_water.html](http://hydroinnova.com/snow_water.html)). Using dual-channel, the system is composed of two detector tubes  
199 filled with  $^{10}\text{BF}_3$ ; one is sensitive to neutrons with a maximum energy of  $\sim 0.025$  eV,  
200 whereas the second is sensitive to moderated energy neutrons from  $\sim 0.2$  eV to 100 keV.  
201 The cosmic ray probe above the snowpack (Fig. 1b) is an attractive SWE measurement  
202 tool because it can provide direct estimates of SWE within a 20 to 40 ha footprint (20 ha  
203 corresponds to a circle of 252 m radius) (Desilets and Zerda, 2013; Schattan et al., 2017).  
204 In contrast, the footprint of a probe that is installed under the snow is limited to a spot  
205 measurement above the sensor (Fig. 1a). While approach (1a) permits measurements of  
206 very thick snow cover ( $> 1000$  mm SWE) (Gugerli et al., 2019), the drawback of approach  
207 (1b) is that it is limited to low SWE measurements (typically  $< 150$  mm SWE) over  
208 homogeneous flat terrain. However, in the Austrian Alps, contrary to previous studies,  
209 Schattan et al. (2017) claim not to have measured saturation for a snowpack of the  
210 order of 600 mm SWE, over an estimated footprint with 230 m radius.

211  
212 The CRNP method requires creating a function for converting neutron counts to snow  
213 water equivalent (Paquet et al., 2008; Gottardi et al., 2013; Sigouin and Si, 2016;  
214 Andreasen et al., 2017; Schattan et al., 2017; Delunel et al., 2014; Bogena et al., 2020).  
215 Desilets (2017) provides the calibration procedure in detail. Neutron counts must be  
216 accumulated over a specified period of time (e.g., from 6 h to 24 h). The CRNP method  
217 requires that the counting rate must first be known (calibrated) and that disturbance  
218 effects on measured cosmic rays at the site location have to be taken into account.  
219 Disturbance effects that need to be corrected include temporal variations in the natural  
220 cosmic-ray flux and variations in air pressure and atmospheric water vapor on site  
221 measurements during the count time. Temporal variation in cosmic-ray flux can be  
222 determined from the NMDB database (Real-Time Database for high-resolution Neutron  
223 Monitor measurements; [www.nmdb.eu](http://www.nmdb.eu)), thereby providing access to reference neutron  
224 monitor measurements from stations around the world. Corrections for air pressure  
225 (linked to the altitude of the station) and atmospheric water vapor variations require  
226 ancillary standard meteorological sensors, which measure atmospheric pressure, air  
227 temperature and relative humidity.



228

229 While accuracy losses that are linked to atmospheric disturbances (pressure and  
230 humidity corrections) are relatively weak (a few percent), this is not the case for primary  
231 variations in the natural cosmic-ray flux (Andreasen et al., 2017), which may drastically  
232 change the results of SWE estimation. This flux can vary up to 30% over long periods  
233 (weeks to months), thereby causing errors up to 50% in SWE estimates when they are  
234 not considered (Paquet and Laval, 2006). Therefore, it is important to correct the  
235 measured signal using the closest world reference station in the vicinity of the  
236 measurement site. If not available, a second cosmic-ray sensor is required to produce  
237 accurate SWE estimates using normalized signals (above and beneath snow) as done by  
238 the Cosmic Ray Detector commercialized by Geonor Inc. ([www.Geonor.com](http://www.Geonor.com)).

239

240 In the case of the second approach, where the probe is installed above the ground  
241 surface (Fig. 1b), the probe must be calibrated for soil moisture. If soil moisture  
242 correction is not applied on the winter signal measurements, retrieved SWE values will  
243 be systematically overestimated. This bias can be corrected using measurements of  
244 CRNP signal without snow, just prior to the onset of snow cover, or using soil moisture  
245 probe during the winter (see Sect. 4).

246

## 247 2.2 Gamma Ray scintillator (GMON)

248 Monitoring snow water equivalent by using natural soil radioactivity is a well-known  
249 approach (Bissell and Peck, 1973). Since 1980, an airborne snow survey program using  
250 this technology has successfully collected areal mean SWE data for operational flood  
251 forecasting over the whole of northwestern North America, including the Rocky  
252 Mountains, Alaska and Great Plains (National Operational Hydrologic Remote Sensing  
253 Center, <https://www.nohrsc.noaa.gov/snowsurvey/>). The mean areal SWE value is  
254 based on the difference between gamma radiation measurements over bare ground and  
255 snow-covered ground, the latter being attenuated by the snowpack (Carroll, 2001).

256

257 The principle of SWE measurements that are based on the Gamma Monitor (GMON) ray  
258 scintillator is the absorption by the water, regardless of its phase (liquid, snow or ice), of  
259 the natural radioactive emission of Potassium-40 ( $^{40}\text{K}$ ) from soils (Ducharme et al.,  
260 2015). This naturally occurring radioactive isotope of potassium has a gamma emission  
261 of 1.46 MeV. The GMON probe also measures the emission of Thallium-208 ( $^{208}\text{Tl}$ ),  
262 which emits gamma rays at a slightly higher energy (2.61 MeV) that originate from the  
263 decay of Thorium 232 (Choquette et al., 2013; Wright, 2013; Strandén et al., 2015). Both  
264 of these elements are common to almost all types of surfaces, regardless of whether  
265 these are organic or non-organic soils. However, we observed that the isotope  
266 associated with the higher count (i.e.,  $^{40}\text{K}$ ) is generally the most reliable.

267

268 The GMON, which is manufactured by Campbell Scientific (Canada) (CS7525;  
269 <http://www.campbellsci.ca/cs725>), is composed of a tube 62 cm long, and 13 cm in  
270 diameter, weighing 9 kg. The experimental set-up, which is illustrated in Fig. 1c, is based  
271 on the initial, snow-free measurement of the number of counts for  $^{40}\text{K}$  or  $^{208}\text{Tl}$  per

272 period of time, which would be later decreased by the presence of the snowpack.  
273 Typically, 300 000 and 60 000 counts per 24 hours for  $^{40}\text{K}$  and  $^{208}\text{Tl}$ , respectively, are  
274 suggested as minimal values to provide accurate SWE measurements (CS725 Snow  
275 Water Equivalent Instruction Manual, 2017, Campbell Scientific [Canada] Corporation,  
276 Edmonton, AB; [https://s.campbellsci.com/documents/ca/manuals/cs725\\_man.pdf](https://s.campbellsci.com/documents/ca/manuals/cs725_man.pdf)). The  
277 observed rate of soil emission at each site allows the operator to define the minimum  
278 sampling time frequency. Seeding experiments conducted using potassium fertilizer  
279 show the potential for increasing potassium counts that are measured by the CS725 by  
280 up to 80% at sites where low counts are found (Wright et al., 2011). As is the case for  
281 ground-pointing CRNP, measuring the base-line signal of the radiation energy emanating  
282 from the ground prior to the first snowfall is a critical step in signal processing, given  
283 that it also depends upon soil moisture (SM) during the winter and spring periods. SM  
284 attenuates the natural dry-ground emission, resulting in an overestimate of SWE during  
285 signal processing when SM increases (Choquette et al., 2013) (see Sect. 4).

286  
287 The CS725-Campbell GMON sensor has been the subject of a detailed performance  
288 analysis within the framework of the WMO Solid Precipitation Intercomparison  
289 Experiment (Smith et al., 2017). Moreover, since the device is sensitive to water  
290 contained in soils, it can be successfully used to estimate soil moisture during snow-free  
291 seasons. An operational GMON network, with a sampling frequency of 6 h, is actually  
292 deployed across the southern part of Québec and Labrador, northeastern Canada (45-  
293 55°N); it accounts for 116 stations that are operated by Hydro-Québec (87), Rio-Tinto  
294 (13), Ministère de l'Environnement et de la Lutte contre les changements climatiques of  
295 the Québec Government (10), Parks Canada (4), and the Government of Newfoundland  
296 and Labrador (2), and which are dedicated to water resource forecasting (Alexandre  
297 Vidal, Hydro-Québec, personal communication, November 2020). Also, these  
298 continuous measurements from the GMON Québec network are demonstrably very  
299 useful for validating the assimilation of microwave observations into a snow model  
300 (Larue et al., 2018). Recently, GMON had also demonstrated its robustness in a research  
301 project on seasonal snow monitoring from a station that was installed at 4962 m asl in  
302 the Nepalese Himalayas (Langtang Valley) to quantify the evolution of SWE (Kirkham et  
303 al., 2019).

### 304 2.3 FMCW radar (FMCW-Radar)

306 The principle of frequency-modulated continuous-wave (FMCW) radar has been well  
307 known since the 1970s (see the review s by Peng and Li, 2019 and by Pomerleau et al.,  
308 2020) and has been popularized for snow studies since Koh et al. (1996), Marshall et al.  
309 (2005), and Marshall and Koh (2008), among others, were published. FMCW-Radar is an  
310 active system design for distance measurements. The radar emits a wave at variable  
311 frequencies that are centered on a reference frequency. When the radar receives a  
312 return from a target, the frequency difference between the emitted and reflected  
313 signals is measured (Fig. 1d). Since the frequency change rate is known, the time  
314 between the emission and the reception of the echo can be measured, z from which the  
315 radar-target distance is calculated.

316

317 The principle of SWE retrieval is based on the time measurement of wave propagation  
318 in the snowpack that is proportional to the snow refractive index (square of  
319 permittivity), which changes the wave-speed propagation. As the refractive index of  
320 snow can be linked to its density (Tiuri et al., 1984; Matzler, 1996; Pomerleau et al.,  
321 2020), SWE can be retrieved knowing the snow depth. The experimental set-up is shown  
322 in Fig. 1d and illustrated in Fig. 2e.

323

324 Two main FMCW-radar specifications are required for SWE measurement: the radar  
325 central frequency and its bandwidth that is scanned. The central frequency specifies  
326 three parameters: a) the loss in signal strength of an electromagnetic wave that would  
327 result from a line-of-sight path through free space (the higher the frequency, the greater  
328 the loss); b) its penetration depth (the higher the frequency, the less penetration power  
329 it has); and c) its sensitivity to liquid water content in the snowpack. The bandwidth  
330 specifies the distance resolution and, thus, the precision: the wider the bandwidth, the  
331 lower the resolution. There is negligible frequency dependency of the snow refractive  
332 index ( $n'$ ), which governs wave propagation in the snowpack. The refractive index ( $n'$ ) is  
333 linked to snow density ( $\rho$ ) by a linear relationship:  $n' = 8.6148 \cdot 10^{-04} \rho + 9.7949 \cdot$   
334  $10^{-01}$  (Pomerleau et al., 2020).

335

336 For snow studies, several FMCW radars with different frequencies and resolutions are  
337 used, such as those common at the X-band (10 GHz), operating over 8–12 GHz  
338 (Ellerbruch and Boyne, 1980; Marshall and Koh, 2008). They provide a vertical resolution  
339 on the order of 3 cm. In contrast, L-Band FMCW radar (1.12–1.76 GHz) allows greater  
340 penetration but suffers from reduced vertical resolution (Yankielun et al., 2004).  
341 Multiband band FMCW radars have also been developed (Rodriguez-Morales et al.,  
342 2014), such as an L/C-band (2–8 GHz) that was used to successfully retrieve snow depth  
343 (Fujino et al., 1985), a C/Ku (8–18 GHz) large wideband FMCW radar that is capable of  
344 detecting crusts as thin as 0.2 mm within the snowpack (Marshall and Koh, 2005), or the  
345 improved (C-, X-, and Ka-band) radar (Koh et al., 1996). Operating frequencies of  
346 commercial, low-cost radar systems, such as those that are adopted for automotive  
347 radar systems (Schneider, 2005), are now available for K-band (24 GHz) and W-band (77  
348 GHz) applications.

349

350 The availability of such new types of lightweight and very compact 24-GHz FMCW radar  
351 systems has motivated our research group to assess their ability to monitor the SWE  
352 continuously and autonomously (Fig. 2e) (Pomerleau et al., 2020). The FMCW-Radar  
353 that is used, which is centered on 24 GHz (K-band), is manufactured by IMST (IMST  
354 sentire™, IMST, Kamp-Lintfort, Germany; <http://www.radar-sensor.com/>); its housing  
355 module is very compact (114.0 mm × 87.0 mm × 42.5 mm) and weighs 280 g. This  
356 FMCW-Radar has a bandwidth of 2.5 GHz, scanning over 23–25.5 GHz, which provides a  
357 resolution of 6 cm in the air. These specifications appear to be a good compromise  
358 between penetration and resolution capabilities for SWE estimation, while keeping the  
359 sensor affordable, light and compact, with low power consumption. The radar

360 penetration depth ( $\delta Pr$ ) of dry snow significantly decreases with density following a  
361 power law, which varies with temperature (see Fig. A2, Pomerleau et al., 2020). At  $T = 0$   
362  $^{\circ}\text{C}$ ,  $\delta Pr$  decreases from 6.78 to 4.81, 3.26 and 2.05 m for respective snow densities of  
363 150, 200, 275 and  $400 \text{ kg m}^{-3}$  (Pomerleau et al., 2020). Wet snow drastically reduces  
364  $\delta Pr$ , given that liquid water strongly absorbs the radar signal, leading to high reflectivity  
365 at the air/wet snow interface and weak transmissivity. For example, the two-way radar  
366 penetration depth decreases abruptly from 2 m for dry snow at a density of  $400 \text{ kg m}^{-3}$   
367 to 0.05 m for wet snow with 0.5% of liquid water content (as a volume fraction). It  
368 should be noted that this strong sensitivity to wet snow allows the radar to precisely  
369 detect the onset of snowpack surface melt, a benefit that is discussed in Sect. 4.

370 One of the main interests of this approach is its potential capacity to estimate SWE from  
371 a small remotely piloted aircraft (RPA). Over the Arctic, snow cover can generally be  
372 characterized as a two-layer snowpack structure, which is composed of a dense wind-  
373 slab layer overlaying a less-dense near at depth (Rutter et al., 2019; Royer et al., 2021).  
374 Thus, assumptions can be made regarding the mean refractive index of each of these  
375 layers, thereby allowing SWE to be estimated (Kramer et al., 2021). Hu et al. (2019) also  
376 showed the usefulness of imaging FMCW synthetic aperture radar onboard the RPA.  
377 Several studies have also shown the potential of FMCW radar for different applications,  
378 such as avalanche studies (Vriend et al., 2013; Okorn et al., 2014; Laliberté et al., 2021),  
379 snow stratigraphy based on successive FMCW echo analyses (Marshall and Koh, 2005;  
380 Marshall et al., 2007), snowpack tomography (Xu et al., 2018), and ice thickness  
381 monitoring (Yankielun et al., 1993; Gunn et al., 2015). Pomerleau et al. (2020) obtained  
382 highly accurate measurements of lake ice thickness using the 24 GHz FMCW radar, with  
383 a root-mean-square difference (RMSD) of 2 cm accuracy up to  $\approx 1$  m ice thickness  
384 (derived from 35 manual in situ measurements).

#### 385 2.4 GNSS receivers (GNSSr)

386 The principle of SWE retrieval based on Global Navigation Satellite System (GNSS)  
387 receivers is to use the signals that are emitted at 1.575 and 1.609 GHz. by the GNSS  
388 satellite constellations. SWE can be related to the carrier phase change that is induced  
389 by the delay caused by the snowpack at ground level. With two static receivers  
390 (standard GNSS antennas), i.e., one placed under the snow and the other above the  
391 snow, carrier phase measurements of both receivers can be compared and SWE derived  
392 using the onboard measurement hardware (Fig. 1e) (Henkel et al., 2018). Comparing  
393 GNSS signal attenuation measurements between the two antennas (below and above  
394 the snowpack) also permits the retrieval of Liquid Water Content (LWC) of the wet snow  
395 (Koch et al., 2019). Snow depth retrieval has been operational for longer, based on  
396 interferometric reflectometry of GNSS signals (see Larson et al. 2009; Larson, 2016).  
397 Steiner et al. (2019) used a slightly simplified retrieval algorithm based on the path delay  
398 estimates of the GPS signals while propagating through the snow cover due to both  
399 refraction at the air-snow interface and decrease in wave velocity in the medium.

400

401 This relatively recent and novel approach has been validated ([Henkel et al., 2018](#);  
402 [Steiner et al., 2018](#); Koch et al., 2019; and [Appel et al., 2020](#)). A system has now been  
403 commercialized by VISTA Remote Sensing in Geosciences GmbH, Munich, Germany  
404 (SnowSense©, <https://www.vista-geo.de/en/snowsense/>). The experimental set-up is  
405 described in Fig. 1e, based on a low cost and lightweight system. In this study, we used  
406 the SnowSense system for monitoring SWE and LWC throughout a winter, together with  
407 other sensors (see Results Sect. 3). We also developed our own system, shown in Fig.  
408 2d.

409  
410 Another promising way to monitor SWE, which is based on the same principle of GNSS,  
411 is the use of powerful satellite transmissions as illumination sources for bistatic radar.  
412 This so-called “Signals-of-opportunity (SoOp)” approach covers a wide range of  
413 frequencies, such as emissions from United States Navy Ultra High Frequency (UHF)  
414 Follow-On (UFO) communication satellites in P-Band frequencies (between 240-270  
415 MHz). From two P-band antennas (one direct and one reflected), Shah et al. (2017)  
416 demonstrated the feasibility of retrieving SWE using the phase change in reflected  
417 waveforms, which is linearly related to the change in SWE. These methods were not  
418 included in this review since they are still in the development stage and not sufficiently  
419 mature to be operational.

### 421 3. Results

422  
423 Continuous and simultaneous recordings of different instruments on different sites  
424 were analyzed to evaluate their behavior in terms of their temporal evolution. Manual  
425 measurements were used to compare the data between them. First (Sect. 3.1 and 3.2),  
426 two experiments we conducted were compared: GMON and CRNP (Sect. 3.2.1); and  
427 GMON, Radar and GNSSr (Sect.3.2.2). A comprehensive literature review and  
428 evaluations of similar sensors are then presented in Sect. 3.3. This later section also  
429 includes uncertainty estimates of our experiments and from this review, which are  
430 synthesized in Table 2.

#### 431 3.1 Experimental sites and methods

432  
433 We compared four instruments at two snow research stations that were located in  
434 Québec (Canada). The first was the SIRENE site (Site Interdisciplinaire de Recherche en  
435 ENvironnement Extérieur), which is situated on the main campus of the Université de  
436 Sherbrooke in a temperate forest environment (45.37°N, -71.92°W, 250 m asl) (Fig. 2d).  
437 The second site is the NEIGE-Forêt Montmorency (NEIGE-FM) research station. The  
438 instruments were located in an open area (Fig. 2e) of the Montmorency experimental  
439 forest (47.32° N; -71.15° W, 640 m asl) of Université Laval (Quebec City), which is in the  
440 boreal forest. The NEIGE-FM snow research station is part of the World Meteorological  
441 Organization (WMO) Global Cryosphere Watch (GCW) Surface Network CryoNet  
442 (<http://globalcryospherewatch.org/cryonet/sitepage.php?surveyid=191>).  
443

444 Two methods were used to obtain in situ manual SWE measurements in the vicinity of  
445 the four SWE-systems: the snowpit (SP) approach; and snow-tube core samplers (see  
446 Kinar and Pomeroy, 2015; [López-Moreno et al., 2020](#)). The SP-based SWE values (in  $\text{mm}$   
447 =  $\text{kg m}^{-2}$ ) were derived from vertical continuous density profiles, which were determined  
448 by weighing snow samples at a vertical resolution of 5 cm (height of the density cutter).  
449 Assuming an accuracy of density cutter measurements of about 9% (Proksch et al.,  
450 2016), the mean relative SWE accuracy from snowpit can be estimated to be of 6–12%.  
451 SWE estimates were also obtained by weighing the extracted core sample of known  
452 diameter ( $\emptyset$ ) and [snow depth](#) using a coring tube. In this study, the core sampling was  
453 performed using three different snow tube models, which were averaged: “Carpenter”  
454 (Federal standard sampler, 3.7 cm  $\emptyset$  tube), the Hydro-Quebec snow tube (12.07 cm  $\emptyset$ ),  
455 and an in-house Université Laval snow tube (15.24 cm  $\emptyset$ ). The [uncertainties](#) of tube core  
456 sampling that we carried out on snowpack up to 600 mm SWE with large tubes is [on](#)  
457 the order of 6%, but can be higher, up to 12%. Such [uncertainty](#) is difficult to define, as  
458 discussed in Sect. 3.3 and in [discussion contained in the Appendix](#). Furthermore, as  
459 manual measurements cannot be taken at the same location [throughout](#) a given winter  
460 period, this could generate uncertainty when compared to a fixed instrument, due to  
461 small-scale spatial variability of SWE and surface roughness ([López-Moreno et al., 2020](#)).  
462

463 The snowpack properties were derived from GMON and CRNP systems throughout the  
464 entire winter season of 2008-2009 (Fig. 3) and from GMON, FMCW-Radar and GNSSr  
465 systems in 2017-2018 (Fig. 4). [The CRNP probe that was used was the same as the  
466 French EDF probe that was placed on the ground \(Paquet et al., 2008\) and installed at  
467 about 5 m distance from the GMON footprint. The GMON was installed on a 2 m mast  
468 above the surface, located in a slight depression in comparison with the terrain where  
469 the CRNP was buried. The CRNP counts were accumulated over 1 hour and normalized  
470 against an identical probe that was installed nearby, just above the snow surface. The  
471 GMON counts were accumulated over 6 hours, and only  \$^{40}\text{K}\$  counts were considered \(TI  
472 counts were similar, but not shown\). The GMON sensor was adjusted to take into  
473 account the soil moisture prior to snowfall accumulation, but not afterwards.](#)  
474

475 In addition to SWE measurements, continuous automatic snow depth measurements  
476 were performed using an [ultrasonic ranging sensor](#) (Campbell Scientific, SR50AT-L), and  
477 manually with a graduated probe around the sampling sites. LWC measurements were  
478 derived from GNSSr (Fig. 4). Air temperature (T) at 2 m height and total daily  
479 precipitation (tipping bucket rain gauge) were recorded at the SIRENE site; a threshold  
480 of  $T = 0^\circ\text{C}$  was used to separate solid and liquid phases.

481 In this section, we present comparisons between these sensors with [manual snowpit](#)  
482 validation data [that were](#) measured as close as possible to the automatic instruments.  
483 [The uncertainty of measurements, including](#) other measurements that we carried out  
484 (not shown), is [reported](#) in Table 2.

485

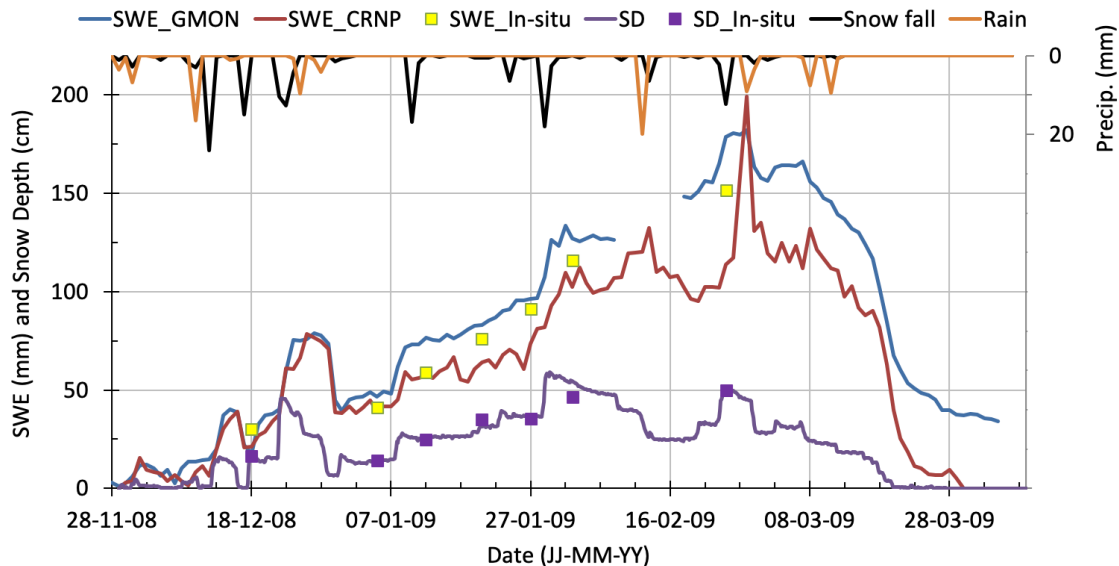
## 486 3.2 Validation of measurements

### 487 3.2.1 Comparison of GMON- and CRNP-derived SWE seasonal evolution

488 Figure 3 shows the SWE evolution of a shallow snowpack (maximum snow depth of 56  
 489 cm) at the SIRENE site that was derived from daily mean values of the GMON and CRNP  
 490 data throughout the winter season of 2008-2009.

491  
 492 Results show that GMON and CRNP evolve similarly over the winter, with GMON SWE  
 493 being slightly higher after the first winter month (SWE > 50 mm). This difference  
 494 occurred after a pronounced melting spell (29-30 December 2008) and is explained by  
 495 the water that has accumulated on the ground under the GMON and not on the CRNP,  
 496 due to the local terrain configuration. The moisture beneath the GMON formed a  
 497 significant ice layer that lasted all winter. As this ice layer was not present in snowpits  
 498 (the amount of water in an ice crust being otherwise difficult to measure), this could  
 499 possibly explain differences between GMON and manual measurements. Precipitation  
 500 (snowfall and rain) is also plotted, showing how GMON and CRNP develop with each  
 501 event. For that given winter, rain-on-snow events were frequent, leading to moisture  
 502 accumulation on the ground. Note also that at the end of the winter, there was ice that  
 503 had not yet melted and water accumulation under the GMON, leading to a significant  
 504 GMON overestimation in terms of snow w.e., but not in terms of total water. There was  
 505 no more snow on the ground after 20 March 2009. The accuracy measurements are  
 506 discussed in Sect. 4.2.

507



508  
 509 Figure 3. GMON- and CRNP-derived snow water equivalent (SWE, mm), snow depth (SD,  
 510 cm), and recorded daily solid and liquid precipitation (Precip., mm, right hand scale), in  
 511 comparison to validation data (in situ) at the SIRENE site for the winter season of 2008-  
 512 2009. Continuous SD measurements (purple line) are from SR-50 and SD\_in situ  
 513 measurements (purple square) are from snowpits. Open yellow squares correspond to  
 514 manual in situ SWE measurements.

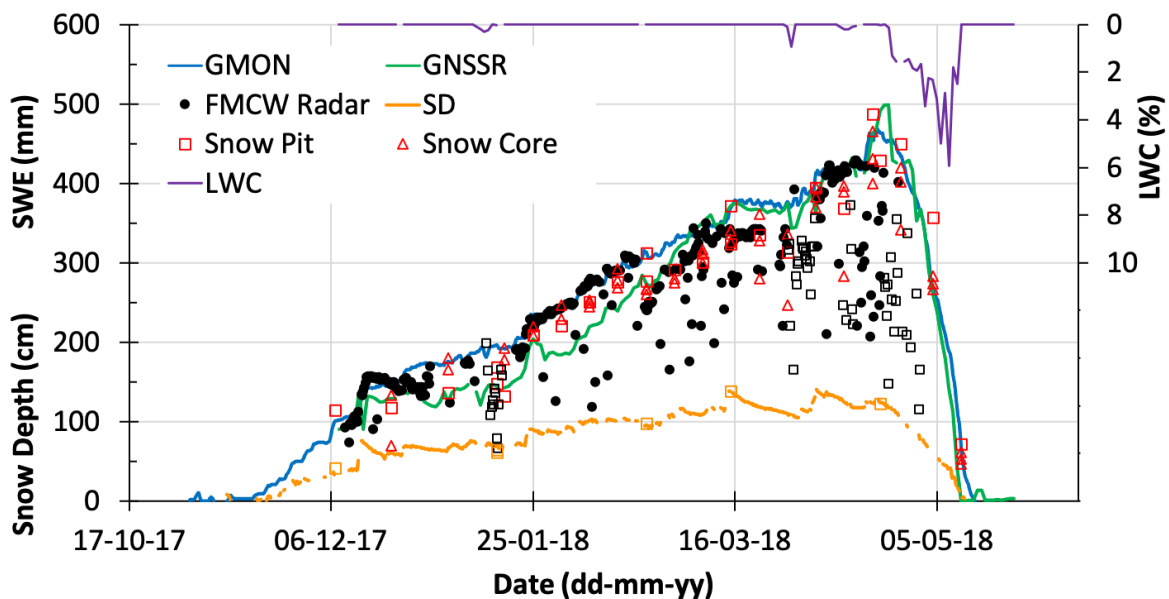
515

516 3.2.2 Comparison of GMON-, Radar- and GNSSr-derived SWE seasonal evolution

517 Figure 4 shows the SWE evolution that was measured by the three instruments: GMON  
 518 ( $^{40}\text{K}$  counts only), FMCW-Radar and GNSSr, which had been placed in close proximity to  
 519 one another at the NEIGE-FM research station for the winter season of 2017-2018. A  
 520 maximum snow depth of 120 cm was measured during the season, corresponding to  
 521 500 mm SWE maximum at the end of April.

522  
 523 The three instruments were compared to manual in situ measurements that had been  
 524 derived from SP (red squares) and core (red triangles) approaches in Fig. 4. We  
 525 distinguished the two methods (SP and snow core) because they exhibit significant  
 526 differences, with a RMSD of 33 mm (12%). These discrepancies are the result of two  
 527 problems: 1) SWE spatial variability, mainly due to snow depth variability (López-  
 528 Moreno et al., 2020); and 2) the method that was used, since the design of snow tubes  
 529 and cutters has some influence on sampling errors and bias (Goodison et al., 1987).  
 530 Therefore, uncertainty analyses (Sect. 3.3) were performed considering manual SP as  
 531 the reference because the SP approach was used for both experiments.

532  
 533



534 Figure 4. GMON- (blue line), FMCW Radar- (black closed circles) and GNSSr-derived  
 535 (green line) snow water equivalent (SWE, mm), snow depth (orange line for SR50AT-L  
 536 data and orange open squares for in situ data) (SD, cm) and GNSSr-derived Liquid Water  
 537 Content (LWC, % volumetric, purple line, right scale), in comparison to in situ snowpit  
 538 (open red square) and snow core (open red triangle) SWE measurements at the NEIGE-  
 539 FM site for the winter season of 2017-2018. For FMCW-Radar data (in black), plain  
 540 circles are for dry snow, while open squares correspond to wet snow.

541  
 542  
 543 The continuous simultaneous recordings from the different instruments permit  
 544 temporal evolution analysis (Fig. 4). During the accumulation period, GMON shows  
 545 relatively smooth and consistent evolution in SWE leading to a maximum of 465 mm on



546 19 April 2018, while the FMCW-Radar time series is more erratic and requires filtering to  
547 remove low SWE outliers. These points are mainly due to incorrect detection of the  
548 peak of the radar echo on the ground (snow-ground interface), sometimes with low  
549 amplitude, and which can be filtered with improved data quality processing of raw  
550 recording (Pomerleau et al., 2020). In particular, all data that were acquired under wet  
551 snow conditions (open black squares, Fig. 4), which correspond to melting periods with  
552 measured air temperature above 0° C, are obviously underestimated as expected,  
553 because of radar wave absorption by liquid water in the snowpack. Compared to the  
554 GMON, the GNSSr signal increases with values that are lower than the GMON until mid-  
555 March at which point it continues to evolve with similar values, as the GMON SWE<sub>max</sub>  
556 of 499 mm w.e. was reached on 23 April 2018. The behavior of the three instruments,  
557 showing different patterns of snow evolution, always remains close to in situ  
558 observations (RMSE compared to the snowpit for GMON and GNSSr are respectively 34  
559 mm and 32 mm; Table 2). It should be noted that in Fig. 4, there is a small difference (+4  
560 days) between the disappearance of snow cover that was recorded with GNSSr (11 May  
561 2018) compared to GMON (14 May 2018). The GNSSr sensor is not sensitive to soil  
562 moisture, while GMON is, despite the instruments being located on a well-drained  
563 sandy site (NEIGE-FM site). In the case shown here, the end of snowmelt is well  
564 captured by both instruments. The accuracy between instruments is analyzed in Sect.  
565 3.4, including a second winter season of continuous measurements at the NEIGE-FM site  
566 (2016-2017, Pomerleau et al., 2020).

567  
568 GNSSr also measures the Liquid Water Content (LWC) of snow (purple line in Fig. 4). The  
569 non-zero LWC values correspond well to positive air temperatures that were recorded  
570 at this site, and also to the drop in FM-Radar measurements (open black squares).

### 571 572 3.3 Analysis of measurement uncertainty

573 It is challenging to compare the accuracy of several instruments, given that there is no  
574 absolute reference for estimating SWE (see Kinar and Pomeroy, 2015). In situ manual  
575 measurements are themselves subject to error, with varying precision depending upon  
576 the method that is being used. Errors are incurred that depend upon the types of  
577 density cutter, tube diameter, sampling quality that is operator dependent, and ice  
578 lenses in the snowpack, among other sources. This is a long-debated topic, with no  
579 actual established international standard protocol (Work et al., 1965; Goodison et al.,  
580 1981, 1987; Kinar and Pomeroy, 2015, López-Moreno et al., 2020). Commonly, the  
581 relative uncertainty for SWE measurement using snow core varies from 6% for shallow  
582 snowpack (0-300 mm w.e.), to 8% (300 – 1000 mm w.e.) for medium snowpack to 10-12  
583 % for deeper snowpack (> 1000 mm w.e.) (see discussion in supplementary data).  
584 Moreover, because manual measurements cannot be taken at the same location during  
585 a given winter period, uncertainty can be introduced by well-known local spatial  
586 variability of snow depth that can occur at fine scales around the sensors. Such  
587 variability depends upon several factors, such as the region and the environment (Arctic  
588 area, aspect and slope in mountainous areas, for example), the micro-topography and  
589 roughness, the vegetation, and snow redistribution by the wind (Clark et al., 2011;

590 Bormann et al., 2013; Rutter et al., 2014; Meloche et al., 2021; Royer et al., 2021).  
591 Furthermore, temporal variability of snowpack snow depth and SWE during the winter  
592 requires regular validation measurements throughout the season.

593 The sensor uncertainties were evaluated from results of our experiments (Sect. 3.2) and  
594 from published studies at other experimental comparison sites (this section). These  
595 other sites are: the Weissfluhjoch high-alpine site near Davos, Switzerland (46.83° N,  
596 9.81° E, 2 536 m asl); Sodankylä, Finland (67.37° N, 26.63° E, 185 m asl); Caribou Creek,  
597 SK, Canada (53.95° N, -104.65°W, 519 m asl); and Fortress Mountain ski area, Kananaskis  
598 Country, Canadian Rocky Mountains, AB (50.82° N, -115.20° W, 2 330 m asl). We also  
599 conducted a series of manual FMCW-radar measurements (e.g., instrument operated by  
600 hand, rather than automatically) over dry snowpack and compared them with in situ  
601 SWE measurements over a wide range of conditions (snow depth and density) in boreal  
602 forest (47° N, 18 points), subarctic taiga (54–56° N, 32 points) and Arctic tundra (69° N,  
603 28 points) environments along a northeastern Canadian transect (Pomerleau et al.,  
604 2020).

605 Note that we only consider here the differences between instruments in the field and  
606 do not address accuracies that were derived from instrument calibration by the  
607 manufacturer.  
608

609 Table 2 summarizes the uncertainties of each instrument and protocol (five cases: CRNP  
610 in and above ground, GMON, FMCW-Radar and GNSSr) in relation to in situ manual  
611 measurements (snowpit method), as well as against snow pillow and snow scale data  
612 that were considered as reference measurements by the authors of the publications  
613 consulted. The results from the COSMOS-UK network (Wallbank et al., 2021) were not  
614 included in the overall uncertainty analysis, because, in this study, depth-based SWE  
615 estimate of fresh snow was used to assess the uncertainty of CRNP ( $R^2$  of 0.53, in the  
616 range of 0-40 mm w.e.). Moreover, soil moisture is usually high and variable in UK,  
617 which acts to increase uncertainties in the SWE estimate (Wallbank et al., 2021).

618 Even if the mechanical method is well known and has been proven over many years, the  
619 snow pillow can sometimes generate large errors when bridging processes occur that  
620 are linked to freeze–thaw cycles leading to disconnection of the weighing mechanism of  
621 the overlying snowpack and the surrounding snowpack (Kinar and Pomeroy, 2015).  
622 However, to compare measurements at a daily scale, they are worth looking at. In Table  
623 2, the uncertainty that relates to the characterization of measurement dispersion  
624 compared to a reference was defined, when known. We used the root-mean-square  
625 difference (RMSD) between an instrument and a given reference, and by a linear  
626 regression over the whole range of measured SWE data that was defined by the  
627 coefficient of determination ( $R^2$ ), the slope and the intercept. The number of points is  
628 also given.

629  
630 Table 2 here

631  
632 Uncertainty analysis does not allow us to determine the “best” instrument, due to the  
633 diversity of experimental conditions, including the range of SWE, the number of

634 experimental sites and point measurements, and [the](#) analyses that are performed over  
635 one or several seasons. It appears that all five methods show [a RMSD in the range of 14](#)  
636 [to 48 mm \(mean 33 ± 11 mm\)](#) against in situ snowpit manual measurements (Table 2).  
637 [This represents a relative value of around 12% on average, depending on the](#)  
638 [instruments.](#) The mean [coefficient of determination for the linear regression](#) is also  
639 [substantially](#) high (mean  $R^2 = 0.92 \pm 0.07$ ). Calculated average slope is  $0.976 \pm 0.13$ ,  
640 meaning that in general, the instruments slightly underestimate SWE for higher SWE  
641 values compared to in situ measurements, even if this is not always the case (Table 2).  
642 RMSD increases slightly when the analysis was performed over a deep snowpack (0–  
643 1000 mm [w.e.](#)) and decreases when compared to another continuous instrument  
644 instead of [manual](#) data (instrument vs GMON and instrument vs snow pillow, average  
645 RMSD =  $23 \pm 10$  mm, Table 2).

646  
647 For the GNSSr instrument that allows the operator to differentiate dry from wet snow,  
648 Koch et al. (2020) have shown that SWE RMSD is about 2.4-fold higher for wet snow  
649 than for dry snow. They did not provide information on LWC uncertainty. In late winter  
650 2021, for very wet melting snow, we did a validation measurement using the WISe A2  
651 Photonic probe (snow liquid-water content sensor that is based on snow microwave  
652 permittivity measurements; <https://a2photronicsensors.com/wise/>). [The GNSSr LWC was](#)  
653 [of 0.44 % \(in volume\) \(the retrieved GNSSr SWE was 149 mm w.e\)](#) and [the LWC from the](#)  
654 [in situ probe was of 0.47 % for the upper half of the snowpack.](#) The [snowpack SWE that](#)  
655 [was measured manually was 133 mm.](#) [The lower half of the snowpack was saturated](#)  
656 [with water.](#) The uncertainty in wet SWE retrieval could result from approximations [in](#)  
657 [the retrieval algorithm that is used.](#) For example, the wet snow refractive index [varies](#)  
658 [linearly with](#) LWC, [with a slope significantly dependent of the snow density \(see the](#)  
659 [appendix of Pomerleau et al., 2020\).](#) This aspect could probably be addressed [further](#) by  
660 improved inversion.

661  
662 The [uncertainty](#) comparison in Table 2 must be weighted according to the analysis  
663 conditions. The accuracy estimates can actually depend upon the number of points  
664 being used and their distribution over time. High inter-annual variability of the  
665 snowpack state (see Bormann et al., 2013; Lejeune et al., 2019) ideally would  
666 necessitate several years of measurements over the winter. The uncertainties of each  
667 GMON and CRNP instrument were derived from huge data sets that were based on  
668 operational networks from the GMON Hydro-Quebec network in Canada and the Alps’  
669 EDF network for the CRNP, respectively, with a very large number of samples taken over  
670 several years of experiments and from multiple sites. The accuracy of the GMON that is  
671 given by the manufacturer is  $\pm 15$  mm for SWE < 300 mm and  $\pm 15\%$  for SWE of 300-600  
672 mm, which is probably rather conservative. [When SWE reference data and site](#)  
673 [adjustment process are well done, the GMON is able to report SWE with an error as low](#)  
674 [as 5% \(Wright, 2011; Choquette et al., 2013; Wright et al., 2013\).](#) The accuracy of the  
675 SnowFox sensor (CRNP) that has been provided by the manufacturer (5-10%) must be  
676 confirmed. The GNSSr approach has recently been the subject of two different  
677 comparative analyses showing very promising results (Henkel et al., 2018; Koch et al.,

2019), which were confirmed by our own results. Over a full season, we obtained an excellent relationship between GNSSr and in situ manual measurements (relative RSMD = 11%, Table 2) and compared with GMON (RMSD = 34 mm, 12%,  $SWE_{GNSSr} = 1.126 SWE_{GMON} - 59.3$ ,  $R^2 = 0.97$ , 153 days).

#### 4. Strengths and Weaknesses of Instruments

In this section, we review the advantages and drawbacks of each of the instruments that are presented, summarized in Table 3. This analysis is based on our experience on instruments and their performances, and a literature review on experimental results of measurements that were carried out with the same approaches. We only consider these field sensors for SWE measurements in terms of their continuous and autonomous capacities, from the perspective of an operational networking context, including criteria regarding low maintenance and relatively easy installation without requiring heavy infrastructure. The four instruments that we analyzed are: CRNP with two experimental setups, i.e., instrument in the ground and above the snow; GMON; 24-GHz FMCW-Radar; and GNSSr (see Table 1 for acronyms and Fig. 1 for the experimental setup). They are all capable of working on batteries and solar panels, by adjusting, if necessary in certain cases, the measurement protocol, i.e. by reducing the frequency of acquisition and on-board data processing. Ten criteria were considered (Table 3): - the SWE<sub>max</sub> capability; - other measured parameters; - whether ancillary data were required for SWE retrieval; - the temporal sampling rate, i.e., whether they were capable of quasi-continuous SWE measurement capability, although the notion of continuous SWE measurements is relative to the application; - the footprint of the sensor, i.e. taken here in the sense of the area from which emanates the measured radiation having interacted with the snow; - the power consumption; - the main strength of the approach; - their critical drawbacks; - the price of the instrument itself, knowing that the cost of the system may vary in case additional instruments are required for the SWE measurements. Also, the cost that is associated with on-site maintenance during winter should be considered here, but in our case, the 4 instruments are considered on the same basis, i.e., autonomous, with no need for intervention; - and the possibility of other applications.

The cost criterion is a very relative argument, which can influence the choice of decision-makers or researchers, depending upon the intended application (e.g., large network, in remote areas, among others) and also on the purchasers.

Table 3 here

To complement the main criteria that are presented in Table 3, we include the following additional considerations, which are reported in the literature, by order of presentation rather than order of merit.

721 The CRNP approach is based on neutron component that has absorption mean free path  
722 about an order of magnitude larger than that for gamma radiation. This makes it the  
723 most efficient system for very deep snowpack analysis (Paquet et al. 2008).  
724 Measurements over a snowpack of up to 2000 mm SWE were performed using the  
725 SnowFox sensor at the UC Berkeley Central Sierra Snow Lab in Soda Springs, CA (2 120 m  
726 asl; <https://vcresearch.berkeley.edu/research-unit/central-sierra-snow-lab>).

727  
728 Regarding CRNP above the snow, Schattan et al. (2017) estimated the theoretical winter  
729 footprint over snow, which they defined as the distance from where neutrons originate.  
730 They found that 86%, 63% and 50% of neutrons originate within respective distances of  
731 273, 102, and 49 m. In practice, the authors found that the average footprint during the  
732 season, based on measurements over almost three snow seasons, was estimated to be  
733 around 230 m, possibly more.

734  
735 Moreover, CRNP is inherently weakly sensitive to interference from vegetation  
736 compared to systems that are based on EM low frequencies (GMON, FMCW-Radar and  
737 GNSSr). This is in part because the attenuation coefficient for fast neutrons ( $\sim 0.01 \text{ m}^{-2}$   
738 kg in water, Murray and Holbert, 2020) is an order of magnitude smaller than the  
739 analogous attenuation coefficient in vegetation for GNSS microwaves (1.5 GHz) (e.g.,  
740 Wigneron et al., 2017). Also, vegetation can itself be a significant source of  
741 electromagnetic emissions (Larson et al., 2014; Wigneron et al., 2017). The CRNP is  
742 affected by all sources of hydrogen within its measurement footprint. As Biomass  
743 increases the hydrogen concentration in the CRNP's footprint, it is possible to monitor  
744 changes in biomass (Vather et al., 2020).

745  
746 The instruments pointing toward the soil, CRNP and GMON above the surface, are  
747 sensitive to soil moisture. This can be a relatively large source of error with these  
748 measurement principles, given that these sensors are interpreting near-surface soil  
749 liquid content as SWE. This is especially the case during spring freshets and mid-season  
750 thaw cycles (see Fig. 3 and Smith et al., 2017). Heavy rainfall on snow also leads to  
751 erroneous SWE estimates due to the occurrence of water ponding beneath the snow  
752 (Fig. 3). Installation on well-drained soils can mitigate these effects, as shown in Fig. 4.  
753 By assuming that soil moisture levels remain stable throughout winter, which can be the  
754 case when soil remains frozen (see Gray et al., 1985, 2011), this soil moisture-induced  
755 bias can be adjusted prior to the first snowfall or one must apply a correction based on  
756 soil moisture conditions that are otherwise known. Based upon 10+ years of experience  
757 with a large GMON network that is deployed in Quebec, Canada, over northern organic  
758 boreal soil, it has been shown that in most cases, SM does not vary substantially during  
759 the winter season (Choquette et al., 2013; Ducharme et al., 2015). To consider SM as  
760 constant, mathematical equations that are used in calculating SWE can be simplified. If  
761 the goal is to measure the total water that is available for hydrological purpose, this  
762 aspect can become an advantage.

763

764 Counter-based sensors such as CRNP and GMON need to accumulate enough counts for  
765 reliable SWE estimates. Thus, it may be necessary to accumulate the counts over an  
766 adjusted period of time (several hours, depending on the case), so that the  
767 measurement is not strictly continuous. This can prevent accurate detection of short  
768 events, sudden heavy snowfalls, for example.

769

770 For the GMON, depending on the type of soil at the measurement site, gamma ray  
771 emissions may not be sufficient and could require a longer integration period, as is the  
772 case for sites with thick organic soil layers. It is possible to enrich gamma emissions by  
773 using bags or pipes of potassium-rich fertilizer, thereby maintaining a shorter  
774 integration time. [Wright et al. \(2011\)](#) achieved success with this approach, [which yielded](#)  
775 [significantly higher count strengths. Such a protocol is illustrated in Fig. 2g \(data not yet](#)  
776 [processed\). Over glaciers, GMON requires such an enriched gamma emission setup. The](#)  
777 [size of the area that is effectively monitored by the GMON \(“footprint”\) extends to 10 m](#)  
778 [from the detector when there is no snow or water on the ground \(Ducharme et al.,](#)  
779 [2015\). The size of the sensed area exponentially decreases with increasing SWE and is](#)  
780 [estimated to be of the order of 5 m radius \(50 – 100 m<sup>2</sup>\) for 150-300 mm w.e. \(Martin et](#)  
781 [al., 2008; Ducharme et al., 2015\). This relatively large foot print is an advantage of this](#)  
782 [sensor.](#)

783

784 With FMCW-Radar technique, as previously stated, penetration depth strongly depends  
785 on the measurement frequency. Generally, high frequency instruments result in higher  
786 resolution measurements, but these are also affected by greater signal attenuation, i.e.,  
787 by a reduced depth of penetration. A disadvantage of this approach is that it requires  
788 the measurement of snow height as close as possible to the radar sensor. Also, the  
789 algorithm for thresholding the radar echo peaks must be developed as well as the  
790 calculation of the SWE (see Pomerleau et al., 2020).

791

792 GNSS electromagnetic waves can be attenuated under the forest canopy, as the forest  
793 transmittivity at 1.5 GHz is not negligible (Wigneron et al., 2017). Yet, because we  
794 normalized the signal beneath the snow against the one acquired above the snowpack,  
795 when both antennas were placed under the canopy, this effect should not alter  
796 retrieval. GNSSr is not well suited to very steep mountainous terrain (e.g., deep-valley  
797 bottoms), given that a rather wide sky-view factor is needed by the instrument, [and](#)  
798 [that this view can be limited in such environments, depending on slope and location \(Koch et](#)  
799 [al., 2019, Steiner et al., 2018\).](#)

800

801 The main conclusions that emerge from Table 3 and the aforementioned remarks are  
802 the following, recalling that each approach has its own advantages and limitations (by  
803 order of presentation rather than by order of merit):

- 804 • [The CRNP approach is based on measurements of natural cosmic ray fluxes, which](#)  
805 [are variable in time, unfortunately requires complementary atmospheric](#)  
806 [measurements \(temperature, pressure and atmospheric humidity\) at each site for](#)  
807 [correcting the signal and must be normalized against a nearby reference site](#)

808 (available worldwide). CRNP on the ground: This is the most efficient system for very  
809 deep snowpack (> 2000 mm w.e., perhaps up to 7000 mm w.e.), as is the case in  
810 mountain environments or northerly areas that are witness to winter lake-effect  
811 snowfall. The most advantageous aspect of the CRNP is its ability to measure SWE  
812 through complex snow layers from shallow to deep snow conditions. This is a robust  
813 and mature approach, as demonstrated by the French EDF experience (Gottardi et  
814 al., 2013; Lejeune et al., 2019); however, the EDF's sensor is based on a system that  
815 is not exploited commercially. The alternative sensors are the CRNP-based sensor  
816 that is manufactured by Hydroinnova (SnowFox or CRS-1000/B, Hydroinnova,  
817 Albuquerque, NM) (<https://hydroinnova.com>) and the CRD manufactured by Alpine  
818 Hydromet ([www.alpinehydromet.com](http://www.alpinehydromet.com)) and marketed by Geonor Inc. These  
819 sensors are relatively new and still need to demonstrate their robustness. The cost  
820 of Hydroinnova system is about 11 000 US\$ for sensor only. As previously  
821 mentioned, ancillary sensors (atmospheric humidity and barometric pressure  
822 sensors) must be added, and the actual price could be up to 17 000 US\$ for full  
823 setup. The cost of the Geonor Inc. system is 15 000 US\$.

- 824 • CRNP above the snow: The most interesting system for measuring SWE over a large  
825 footprint, but it is limited to shallow snowpacks. It is the only approach that can  
826 provide an integrated spatial measurement. This approach also needs appropriate  
827 adjustment for each site in terms of soil moisture corrections, which can be difficult  
828 over a large area.
- 829 • GMON: This is one of the most mature instruments for snowpacks that are not too  
830 deep (600 mm w.e. according to manufacturer specifications, but up to 800 mm w.e  
831 based on our experience), with a medium footprint (10 m). Yet, it needs systematic  
832 site adjustment for soil moisture-induced error, which can increase the bias of  
833 measurements, particularly at the end of the winter when the soil becomes  
834 potentially saturated during snowmelt. It is the most expensive of the four  
835 instruments (around 16 600 US\$, 20 000 \$CAD). This system has proved its  
836 robustness and accuracy within the operational Hydro-Quebec Canadian network  
837 over a wide variety of environments for almost 10 years (Choquette et al., 2013).
- 838 • FMCW-Radar: This approach requires the measurement of the snow depth to be  
839 able to retrieve SWE. Its weak point is its limitation in measuring the SWE of wet  
840 snow. Yet, the instrument is very useful for dry snowpack characterization, in terms  
841 of stratigraphy or for avalanche studies, and also for detection of snowmelt events.  
842 Moreover, it is not expensive (1 000 US\$, 800 €). As it is very light weight and  
843 compact, one of its strengths is its potential capability to retrieve SWE from  
844 remotely piloted aircraft above arctic snowpacks.
- 845 • GNSSr: The potential of the GNSSr approach, which is a light and compact system, is  
846 strong, given its capability of measuring SWE and LWC with high accuracy, and to  
847 derive snow depth. For SWE retrieval, its performance remains very good (relative  
848 RSMSD of ~10% in the range of 0-1000 mm) and has the capacity to measure deep  
849 snowpack (up to 1 500 mm w.e.). SWE accuracy for wet snow has yet to be  
850 improved, as it depends upon the GNSS signal processing. Its cost is 8 550 US\$ (7 000

851 Euros). The station includes the software/license and processing is performed  
852 onboard of the station. The Station comes with 1 year of Iridium communication for  
853 retrieved product SWE/LWC (via VISTA). VISTA supports customer to find  
854 operational way to retrieve data in operational use for future. The license alone for  
855 processing the raw data can also be directly purchased at ANavS  
856 (<https://anavs.com/>) for 2 370 US\$ (2 000 €).

## 857 858 **5. Conclusions**

859  
860 In this paper, we evaluated four types of non-invasive sensors that have all reached a  
861 certain level of maturity enabling deployments of autonomous networks for monitoring  
862 water equivalent of snow cover (SWE). These include the Cosmic Ray Neutron probe  
863 (CRNP), the Gamma Ray Monitoring (GMON) sensor, the frequency-modulated  
864 continuous-wave radar at 24 GHz (FMCW-Radar), and the Global Navigation Satellite  
865 System receiver (GNSSr) (see Table 1). This new generation of light and practical systems  
866 that are based on radiation-wave measurement is now commercially available. The  
867 GMON is already operationally used in Québec, Canada, for hydrological purposes  
868 (Hydro-Québec, Rio-Tinto, and governments).

869  
870 The analysis of their performances that are summarized in Tables 2 (uncertainties of  
871 measurement) and 3 (pros and cons) show that each approach has its strengths and  
872 weaknesses. The synthesis of their advantages/disadvantages shows that the overall  
873 uncertainties remain in the range of manual measurements, i.e., 9 to 15%. CRNP that is  
874 placed in the ground beneath the snow is the only system capable of measuring very  
875 deep snowpacks, while the GNSSr sensor is limited to SWE up to ~1500 mm w.e., and  
876 the two others up to ~800 mm w.e.. Both CRNP and GMON approaches need  
877 systematic site adjustments for soil moisture characterization. In addition to SWE, an  
878 advantage of the sensor to be considered is their ability to measure other parameters,  
879 such as snowpack stratigraphy for the FMCW-Radar, and the liquid water content for  
880 the GNSSr. The GNSSr approach, which has relatively low cost and is light and very  
881 compact, appears to have a great potential in remote and difficult to access areas.

882  
883 The requirement of automatic instrumentation networks for SWE measurements to  
884 improve seasonal snowpack monitoring is important for several applications, ~~such as~~  
885 where spatially distributed SWE instruments are needed in remote and mountainous  
886 areas, for operational water resource and flood management over snow-driven  
887 watersheds. Networks of continuous SWE measurements are also required for  
888 calibrating satellite-derived SWE information, or for winter transportation safety. This  
889 review of continuous-monitoring SWE sensors is intended to help researchers and  
890 decision makers choose the one system that is best suited to their needs.

## 891 892 **Acknowledgements**



921 We acknowledge all of the students who have contributed to the field measurements,  
922 including Amandine Pierre, Maxime Beaudoin-Galaise and Benjamin Bouchard from  
923 Université Laval, and Patrick Pomerleau, Fannie Larue and Alex Mavrovic from  
924 Université de Sherbrooke. We thank for their support, the staff from Forêt  
925 Montmorency and from the Université de Sherbrooke: Patrick Cliche, Patrick Ménard  
926 and Gabriel Diab. We also thank Alexandre Vidal, Hydro-Québec, and Vincent Fortin,  
927 Environment and Climate Change (ECCC). Finally, the reviewers, together with the  
928 following individuals, are thanked for their helpful comments, which improved the  
929 article: Craig Smith, ECCC; Charles Fierz, SLF, Davos; Yves Choquette, formerly of IREQ-  
930 Hydro-Québec; Florian Appel, VISTA; and ~~and~~ Reinhard Kulke, IMST. W.F.J. Parsons  
931 English language revision.

932

933

934 **Funding:**

935 This project was funded by the Natural Sciences and Engineering Research Council of  
936 Canada (NSERC), the Canadian Foundation for Innovation (CFI), Environment and  
937 Climate Change Canada (ECCC), and Fonds de recherche du Québec – Nature et  
938 technologies (FQRNT), Government of Quebec. The European Space Agency (ESA)  
939 contributes to the installation of the GNSSr sensor within the ESA business development  
940 demonstration project SnowSense (<https://business.esa.int/projects/snowsense-dp>).

941

942 **Conflicts of interest:**

943 The authors declare absolutely no conflicts of interest or business relationships with any  
944 of the manufacturers that are mentioned in this article. The mention of commercial  
945 companies or products does not constitute a commercial endorsement of any  
946 instrument or manufacturer by the authors.

947

948

Table 2 **Uncertainty** analysis for the 4 systems **that were** considered. The Range measurement indicates the highest SWE (mm) value on which the analysis was performed. RMSD: Root Mean Square Difference.  $R^2$  is the determination coefficient of the linear regression analysis. Pts: number of in situ manual samples. “-“ means no information available.

Sensor	Reference data	SWE <sub>max</sub> (mm)	Uncertainty RMSD (mm) (relative RMSD), $R^2$ (slope, intercept)	References, sites, number of points
CRNP in the ground	Manual snowpit	200	14 mm, $R^2 = 0.96$ (0.78, 8.5 mm)	This study (Fig. 3), 7 pts
	GMON	200	28 mm, $R^2 = 0.89$ (0.79, -3.9 mm)	This study (Fig. 3), 2008-2009 season
	Manual snowpit	1700	–, $R^2 = 0.98$ (0.99, 2.8 mm)	Gottardi et al. (2013) EDF system, Alps and Pyrénées 320 year.sites, 1037 pts.
	Snow core	2500	– (2% ± 13%), $R^2 = 0.943$ (–, –)	Gugerly et al. (2019), Glacier de la Plaine Morte, Switzerland, 9 pts (2 winters)
	–	–	5 – 10%	Hydroinnova snowFox <sup>1</sup>
<b>CRNP above snow</b>	–	–	5 – 10%	Hydroinnova CRS-1000/B <sup>2</sup>
GMON	Manual snowpit	500	34 mm (12%), $R^2 = 0.93$ (0.997, 17.1 mm)	This study (Fig. 3 and 4) and Pomerleau et al. (2020), SIRENE et NEIGE-FM, 64 pts
	Snow core	200	40 mm, $R^2 = 0.92$ (1.16, 16.8 mm)	Smith et al., 2017, Sodankylä, Finland, 30 pts
	Snow core	125	23 mm, $R^2 = 0.90$ (0.904, 27.5 mm)	Smith et al., 2017, Caribou Creek, Canada, 19 pts
	Snow core	700	48 mm, $R^2 = 0.92$ (0.881, 32.4 mm)	Smith et al., 2017, Fortress Mountain, Canada, 8 pts
	–	0-300 300-600	±15 mm ±15%	Campbell Scientific CS725 manual <sup>3</sup>
FMCW-Radar 24 GHz	Manual snowpit	500	38 mm (14%), $R^2 = 0.73$ (0.80, 65.0 mm)	This study (Fig. 4) and Pomerleau et al., 2020, 46 pts, dry snow
	Manual snowpit	750	59 mm (30%), $R^2 = 0.87$ (0.98, 0)	Pomerleau et al., 2020, manual measurements, multi sites Northern Québec, Canada, 78 points dry snow
GNSSr	Manual snowpit	500	32 mm (11%), $R^2=0.93$ (1.05, -7.9 mm)	This study (Fig. 4), 18 points
	Manual snowpit	2000	± 15 mm	SnowSense Vista Inc. manual <sup>4</sup> , good conditions
	Manual snowpit	700	23 mm, $R^2 = 0.995$ (0.98, 5.52 mm)	Henkel et al. 2018, Weissfluhjoch, Switzerland (CH)
	Snow-pillow	700	11 mm, $R^2 = 0.999$ (1.01, 1.97 mm)	
	Combined data	800	66 mm, $R^2 = 0.99$ (1.1, -26 mm)	Steiner et al., 2018, Weissfluhjoch, CH, 633 pts
	Manual snowpit	1000	45 mm, $R^2 = 0.98$ (0.98, 31.4 mm) 103 mm, $R^2 = 0.86$ (0.88, 67.3 mm)	Koch et al., 2019 dry snow, Weissfluhjoch, 3 winters Koch et al., 2019 wet snow, Weissfluhjoch, 3 winters
	Snow-pillow and snow scale	1000	30 mm, $R^2 = 0.99$ (0.97, 30.5 mm) 72 mm, $R^2 = 0.93$ (0.92, 65.0 mm)	Koch et al., 2019 dry snow, Weissfluhjoch Koch et al., 2019 wet snow, Weissfluhjoch

1 [https://hydroinnova.com/\\_downloads/snowfox\\_v1.pdf](https://hydroinnova.com/_downloads/snowfox_v1.pdf), Hydroinnova, Albuquerque, NM

2 Hydroinnova, Albuquerque, NM; [http://hydroinnova.com/snow\\_water.html](http://hydroinnova.com/snow_water.html)

3 Campbell Scientific (Canada) Corporation, CS725 manual, [https://s.campbellsci.com/documents/ca/manuals/cs725\\_man.pdf](https://s.campbellsci.com/documents/ca/manuals/cs725_man.pdf).

4 <https://www.vista-geo.de/en/snowsense/>

Table 3 Pro and Cons of the four systems that were considered for SWE monitoring. SM: Soil Moisture. FOV: Field-of-View. The approximate price is given (2021), subject to change according to exchange rate fluctuations.

Sensors	CRNP		GMON	FMCW-Radar 24 GHz	GNSSr
	CRNP on the ground	CRNP above the snow			
<b>SWE<sub>max</sub></b>	<u>Up to</u> 2000 mm	~150-300 mm	<u>600</u> mm <u>(possibly 800 mm)</u>	~1000 mm	<u>Up to</u> 1500 mm
<b>Other measured parameters</b>	-	SM	SM	Melt detection	<u>LWC, SD (estimated)</u>
<b>Other sensors needed</b>	P, T <sub>air</sub> , RH	P, T <sub>air</sub> , RH	-	SD	-
<b>Typical sampling rate</b>	Discontinuous <sup>a</sup>	Discontinuous <sup>a</sup>	Discontinuous <sup>a</sup>	Continuous	Not strictly continuous <sup>b</sup>
<b>Footprint</b>	~1 - 2 m <sup>2</sup>	20-40 ha (300 000 m <sup>2</sup> )	FOV 60° Typically, 50-100 m <sup>2</sup> *	FOV ±32.5° azimuth and ±12° elevation, 0.4 m <sup>2</sup> *	~1 m <sup>2</sup>
<b>Price (US\$, 2021)</b>	Hydroinnova: 11 000 (sensor only) EDF: Not marketed (on request) <sup>c</sup>		16 600 (sensor only)	1 000 (radar and software <sup>d</sup> )	8 550 (complete station <sup>e</sup> )
<b>Power consumption</b>	<u>0.02 W, 12 V DC</u>		<u>0.18 W, 12 V DC</u>	<u>Operating: 8.14 W, 15 V DC</u>	<u>Operating 5 W, 12 V DC</u>
<b>Main advantage</b>	Very deep snowpack	Large footprint	Medium footprint	<u>Snowpack microstructure</u> Very light and compact Low cost	<u>Light</u> SD and LWC Low cost <u>(license only)</u>
<b>Main inconvenience</b>	SM issue Needs ancillary measurements	SM knowledge needed, Needs ancillary measures Shallow snowpack	SM knowledge needed	Dry snow only	Large sky view factor required
<b>Other drawbacks</b>	EDF system not commercially available	<u>Need further validation</u>	<u>Cost</u>	Not turnkey Issue with ice crust	SWE for wet snow must be improved Retrieval algo. issue
<b>Main applications, Capability (see text) Comments</b>	Hydrology Network operational by EDF <sup>c</sup>	Hydrology, SM	Hydrology, SM Network operational by Hydro-Québec	SM, Stratigraphy, Avalanche, Melting monitoring Lake ice thickness RPA capability <sup>f</sup>	Hydrology, SM Avalanche, Melt monitoring

a: Counts must be accumulated over a specified period, e.g. 6h, 12h, or longer. b: GNSS signals must be averaged over a period of time for noise reduction; the typical measurement cycle: 1 per day (possibly up to 6 per day). c: System based on a sensor that is not commercialized. d: Software for sensor settings and reading/recording data, but not for SWE retrievals. e: Subscription license required. f: Remotely Piloted Aircraft capability.

\* Depending on the height of the sensor on its support mast above snow, Field-of-View (FOV) given for 3 m mast.

## Appendix or Supplementary data

### Estimating the uncertainty of in-situ field measurements

In situ field measurements of ~~Snow Water Equivalent~~ (SWE) are accompanied by uncertainties from a variety of sources, which include: 1) instrumental: size and type of sampling tube according to snow depth, weight scale; 2) sampling technique, extracting the snow core; 3) error that is induced by observer; 4) snow conditions: local natural variability, ice lenses and hard snow crusts within the snowpack; 5) soil conditions: irregular soil surface, identification of snow-ground interface. Snow depth is sometimes difficult to estimate over a thawed organic snow-ground interface because surface organic material is often taken into account in the snowpack depth estimate using a snow height probe.

In general, the uncertainty in the SWE depends mainly upon the diameter of the snow core according to the snow depth (the deeper the snow, the smaller the snow core that is required). Few studies discuss the accuracy of in-situ SWE measurements comprehensively over a large range of conditions, from 100 to more than 2 000 mm w.e. For example, the standard protocol that is implemented by Environment and Climate Change Canada is to attain five to ten measurements along a pre-determined survey line of about 150 to 300 m using a translucent plastic ESC-30 sampler (6.2 cm Ø, which is commonly employed in Canada) (Brown et al., 2019). Each study is generally focused on one type of snowpack. Commonly, relative uncertainty varies from 6% for shallow snowpack (0-300 mm w.e.) to 8% (300 – 1000 mm w.e.) for medium snowpack to 10-12 % for deeper snowpack (> 1000 mm w.e.) (see references in the recent review by López-Moreno et al., 2020; also see Work et al., 1965; Turcan and Loijens, 1975; Peterson and Brown, 1975; Goodison et al., 1981 and 1987; Sturm et al., 2010; Berezovskaya and Kane, 2007; Dixon and Boon, 2012; Stuefer et al., 2013; Steiner et al., 2018; Gugerli et al., 2019; Brown et al., 2019). Among recent studies, Stuefer et al. (2013) and López-Moreno et al. (2020) are limited to shallow Arctic snowpack, Steiner et al. (2018) to medium snowpack (up to 1200 mm w.e.), while Gugerli et al. (2019) discuss the problem across a large SWE range of alpine snowpacks over a glacier from 200 to 2300 mm w.e., but with the same snow core (Fig. A1).

In summary, it is well known that SWE uncertainty decreases for shallow snowpack with a larger snow core diameter (typically above 6 cm diameter), given that a larger volume of snow is sampled, Yet, on the other hand, the coring technique is more difficult when snow depth increases. For thicker snowpack, it requires the digging of a pit, because a larger core diameter impeded the retrieval of the snow sample directly from the top of the snow surface. Thus, a large snow core is limited to shallow snowpacks (snow depth less than 1.5 – 2 m). Moreover, commonly remarks from both our experience and the above cited studies agree in that uncertainties in SWE estimates increase with thicker snowpacks. A small diameter snow core is required for thick snowpacks (snow depth above 2 m).

Figure A2 illustrates the underestimation of SWE with a large diameter snow core when SWE increases, from a large dataset that was derived from our International Polar Year experiments (Langlois et al., 2010).

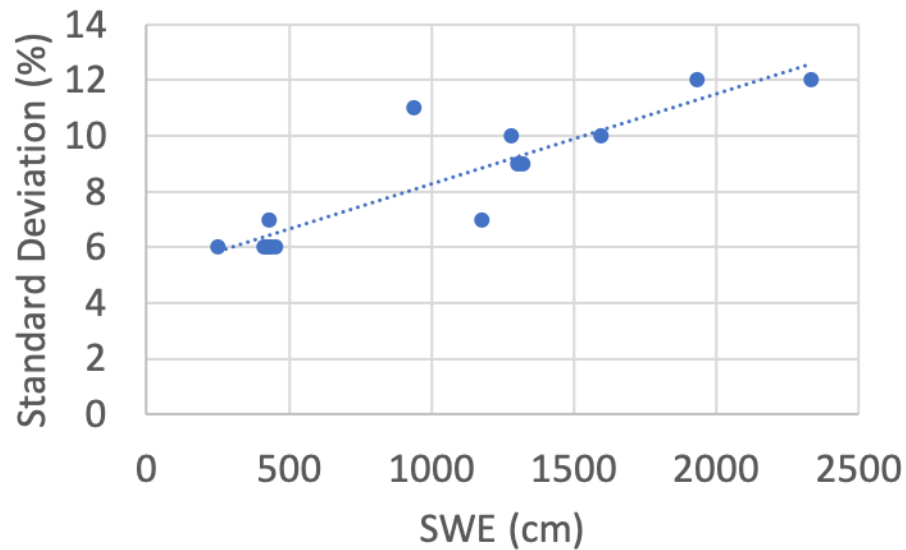


Figure A1 Relationship between the standard deviation (%) of SWE measurements as a function of SWE (mm) based on snow core, derived from Gugerli et al. (2009) (data from Glacier de la Plaine Morte, Switzerland.). Results show an uncertainty of 6 % for SWE of the order of 250 – 500 mm, about 10% for SWE between 1000 and 1500 mm, and 12% for SWE between 2000 – 2500 mm.

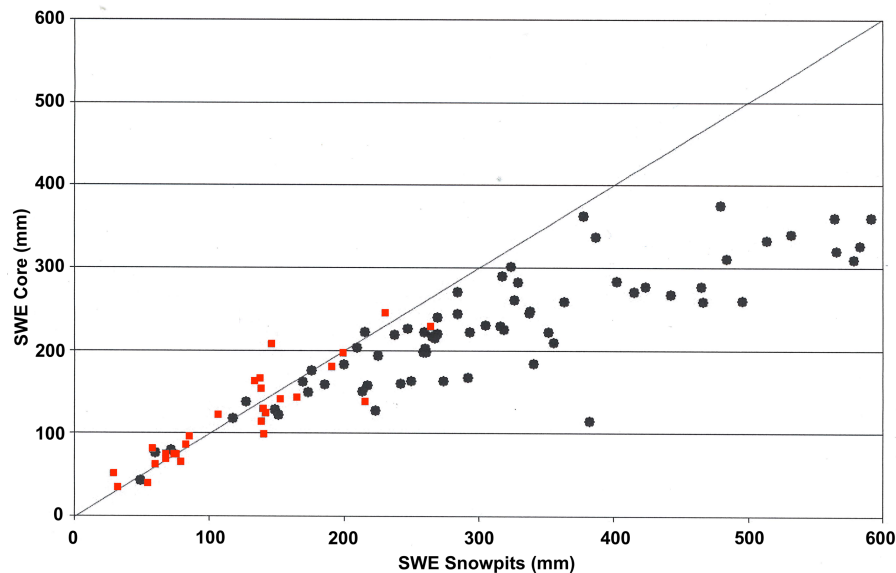


Figure A2. Comparison between SWE measurements (in mm) from snow core and snowpit methods. Red squares are for small diameter snow core (ESC-30 type core: 6.2 cm) and black points are for large diameter snow cores (9.5 cm). The black line is  $Y=X$ . Measured SWE Core values are clearly underestimated above 250-300 mm SWE. Unfortunately, no measurements with small diameter snow cores above 280 mm SWE are present in this example. The database (94 points) is derived from the International Polar Year project (Langlois et al., 2010), including sampling sites at Sherbrooke (SIRENE, 45.37° N; -71.92° W), Sept-Iles (50.30° N; -66.28° W), Schefferville (54.90° N; -66.70° W) and Kuujuaq (58.06° N; -71.95° W) (also see Royer et al., 2021).

## References

For references related to a sensor, the name of the sensor has been highlighted in **bold**.

- Alonso, R., Pozo, J.M.G.d., Buisán, S.T., and Álvarez, J.A.: Analysis of the Snow Water Equivalent at the AEMet-Formigal Field Laboratory (Spanish Pyrenees) during the 2019/2020 winter season using a Stepped-Frequency Continuous Wave Radar (SFCW), *Remote Sens.*, 13, 616. <https://doi.org/10.3390/rs13040616>, 2021. (**SFCW radar**)
- Andreasen, M., Jensen, K. H., Desilets, D., Franz, T., Zreda, M., Bogena, H., and Looms, M.C.: Status and perspectives of the cosmic-ray neutron method for soil moisture estimation and other environmental science applications. *Vadose Zone J.*, 16, 1–11. doi: 10.2136/vzj2017.04.0086, 2017. (**CRNP**)
- Appel, F., Koch, F., Rösel, A., Klug, P., Henkel, P., Lamm, M., Mauser, W., and Bach, H.: Advances in Snow Hydrology Using a Combined Approach of GNSS In Situ Stations, Hydrological Modelling and Earth Observation—A Case Study in Canada. *Geosciences*, 9, 44. <https://doi.org/10.3390/geosciences9010044>, 2019. (GNSSr)
- Berezovskaya, S. and Kane, D. L.: Strategies for measuring snow water equivalent for hydrological applications: Part 1, accuracy of measurements. Proceedings of 16th Northern Research Basin Symposium, Petrozavodsk, Russia, 22–35, 2007. (**Snow core**)
- Bissell, V.C., and Peck, E.L.: Monitoring snow water equivalent by using natural soil radioactivity. *Water Resour. Res.*, 9, 885–890, 1973. (**GMON**)
- Bogena, H.R., Herrmann, F., Jakobi, J., Brogi, C., Ilias, A., Huisman, J.A., Panagopoulos, A., and Pinaras, V.: Monitoring of Snowpack Dynamics with Cosmic-Ray Neutron Probes: A Comparison of Four Conversion Methods. *Front. Water*, 2, 19, doi: 10.3389/frwa.2020.00019, 2020. (**CRNP**)
- Bormann, K.J., Westra, S., Evans, J.P., and McCabe, M.F.: Spatial and temporal variability in seasonal snow density. *J. Hydrol.*, 484, 63–73, 2013. (**Snow core**)
- Brown, R.D., Fang, B., and Mudryk, L.: Update of Canadian Historical Snow Survey Data and Analysis of Snow Water Equivalent Trends, 1967–2016, *Atmosphere-Ocean*, DOI: 10.1080/07055900.2019.1598843, 2019. (**Snow core**)
- Brown, R.D., Smith, C., Derksen, C., and Mudryk, L.: Canadian In Situ Snow Cover Trends for 1955–2017 Including an Assessment of the Impact of Automation, *Atmosphere-Ocean*, DOI: 10.1080/07055900.2021.1911781, 2021.
- Carroll, T. R.: Airborne Gamma Radiation Snow Survey Program: A user's guide, Version 5.0. National Operational Hydrologic Remote Sensing Center (NOHRSC), Chanhassen, 14, <https://www.nohrsc.noaa.gov/snowsurvey/>, 2001. (**GMON**)
- Choquette, Y., Ducharme, P., and Rogoza, J.: CS725, an accurate sensor for the snow water equivalent and soil moisture measurements, in: Proceedings of the International Snow Science Workshop, Grenoble, France, 7–11 October 2013, 2013 (**GMON**)
- Clark, M. P., Hendrikx, J., Slater, A. G., Kavetski, D., Anderson, B., Cullen, N. J., Kerr, T., Hreinsson, E. Ö., and Woods, R. A.: Representing spatial variability of snow water equivalent in hydrologic and land-surface models: A review, *Water Resour. Res.*, 47, W07539, doi:10.1029/2011WR010745, 2011.
- Delunel, R., Bourles, D. L., van der Beek, P. A., Schlunegger, F., Leya, I., Masarik, J. and Paquet, E.: Snow shielding factors for cosmogenic nuclide dating inferred from long-term neutron detector monitoring, *Quat. Geochronol.*, 24, 16–26, doi:10.1016/j.quageo.2014.07.003, 2014. (**CRNP**)
- Desilets, D., and Zreda, M.: Footprint diameter for a cosmic-ray soil moisture probe: Theory and Monte Carlo simulations, *Water Resour. Res.*, 49, 3566–3575, 2013. (**CRNP**)
- Desilets, D., Zreda, M., and Ferré, T.P.A.: Nature's neutron probe: Land surface hydrology at an elusive scale with cosmic rays, *Water Resour. Res.*, 46, 1–7, 2010. (**CRNP**)
- Desilets, D.: Calibrating a non-invasive cosmic ray soil moisture probe for snow water equivalent, *Hydroinnova Technical Document 17-01*, doi:10.5281/zenodo.439105, 2017. (**CRNP**)
- Dixon, D., and Boon, S.: Comparison of the SnowHydro snow sampler with existing snow tube designs. *Hydrologic Processes*, 20, 2555–2562, DOI: 10.1002/hyp.9317, 2012. (**Snow core**)
- Dong, C.: Remote sensing, hydrological modeling and in situ observations in snow cover research: A review. *J. Hydrol.*, 561 (2018) 573–583, 2018.
- Ducharme, P., Houdayer, A., Choquette, Y., Kapfer, B., and Martin, J. P.: Numerical Simulation of Terrestrial Radiation over A Snow Cover. *J. Atmos. Ocean. Technol.*, 32, 1478–1485, 2015. (**GMON**)
- Ellerbruch, D., and Boyne, H.: Snow Stratigraphy and Water Equivalence Measured with an Active Microwave System. *J. Glaciol.* 26, 225–233, 1980. (**FMCW-Radar**)

- [Evans, J. G., Ward, H. C., Blake, J. R., Hewitt, E. J., Morrison, R., Fry, M., Ball, L. A., Doughty, L. C., Libre, J. W., Hitt, O. E., Rylett, D., Ellis, R. J., Warwick, A. C., Brooks, M., Parkes, M. A., Wright, G. M. H., Singer, A. C., Boorman, D. B., and Jenkins, A.: Soil water content in southern England derived from a cosmic-ray soil moisture observing system - COSMOS-UK. \*Hydrological Processes\*, 30\(26\), 4987–4999. <https://doi.org/10.1002/hyp.10929>, 2016.](#)
- Fujino, K., Wakahama, G., Suzuki, M., Matsumoto, T., and Kuroiwa, D.: Snow stratigraphy measured by an active microwave sensor. *Ann. Glaciol.*, 6, 207–210, 1985. **(FMCW-Radar)**
- [GCOS-WMO: The global observing system for climate: implementation needs, World Meteorological Organization, Geneva, Switzerland, 2016. <https://public.wmo.int/en/programmes/global-climate-observing-system>](#)
- Goodison, B., Ferguson, H., and McKay, G.: Measurement and data analysis, in handbook of snow: principles, processes, management, and use, Pergamon press Canada, Toronto, Canada, 191-274, 1981. **(Snow core)**
- Goodison, B.E., Glynn, J.E., Harvey, K.D., and Slater, J.E.: Snow Surveying in Canada: A Perspective, *Can. Water Resour. J.*, 12:2, 27-42, DOI: 10.4296/cwrj1202027, 1987. **(Snow core)**
- Gottardi, F., Carrier, P., Paquet, E., Laval, M.-T., Gailhard, J., and Garçon, R.: Le NRC: Une décennie de mesures de l'équivalent en eau du manteau neigeux dans les massifs montagneux français. In Proceedings of the International Snow Science Workshop Grenoble, 7–11 October 2013, 926–930, 2013. **(CRNP)**
- [Gray, D. M., Granger, R. J., and Dyck, G. E.: Over winter soil moisture changes, \*Transactions of ASAE\*, 28, 442–447, 1985.](#)
- [Gray, D. M., Toth, B., Zhao, L., Pomeroy, J. W., and Granger, R. J.: Estimating areal snowmelt infiltration into frozen soils, \*Hydrol. Process.\*, 15, 3095–3111, 2001.](#)
- GPRI brochure: GAMMA Portable Radar Interferometer (GPRI) [https://gamma-rs.ch/uploads/media/Instruments\\_Info/gpri2\\_brochure\\_20160708.pdf](https://gamma-rs.ch/uploads/media/Instruments_Info/gpri2_brochure_20160708.pdf), 2021. **(Radar)**
- Gugerli, R., Salzmann, N., Huss, M., and Desilets, D.: Continuous and autonomous snow water equivalent measurements by a cosmic ray sensor on an alpine glacier, *The Cryosphere*, 13, 3413–3434, <https://doi.org/10.5194/tc-13-3413-2019>, 2019. **(CRNP and Snow core)**
- Gunn, G.E., Duguay, C.R., Brown, L.C., King, J., Atwood, D., and Kasurak, A.: Freshwater Lake Ice Thickness Derived Using Surface-based X- and Ku-band FMCW Scatterometers. *Cold Reg. Sci. Technol.*, 120, 115–126, 2015. **(FMCW-Radar)**
- Henkel, P., Koch, F., Appel, F., Bach, H., Prasch, M., Schmid, L., Schweizer, J., and Mauser, W.: Snow water equivalent of dry snow derived from GNSS Carrier Phases. *IEEE Trans. Geosci. Remote Sens.*, 56(6), 3561–3572. <https://doi.org/10.1109/TGRS.2018.2802494>, 2018. **(GNSSr)**
- Hu, X., Ma, C., Hu, R., and Yeo, T. S.: Imaging for Small UAV-Borne FMCW SAR. *Sensors*, 19, 87, doi: 10.3390/s19010087, 2019. **(FMCW-Radar)**
- IMST: IMST sentireTM Radar Module 24 GHz sR-1200 Series User Manual. Available online: <http://www.radar-sensor.com/>, 2021 **(FMCW-Radar)**
- Jitnikovitch, A., Marsh, P., Walker, B., and Desilets, D.: Cosmic-ray neutron method for the continuous measurement of Arctic snow accumulation and melt, *The Cryosphere Discuss.* [preprint], <https://doi.org/10.5194/tc-2021-124>, in review, 2021. **(CRNP)**
- Key, J., Goodison, B., Schöner, W., Godøy, Ø., Ondráš, M., and Snorrason, Á.: A Global Cryosphere Watch. *Arctic*, 68, 1, 48 – 58 . <http://dx.doi.org/10.14430/arctic4476>, 2015.
- [Key, J., Schöner, W., Fierz, C., Citterio, M., and Ondráš, M.: Global Cryosphere Watch \(GCW\) implementation plan, World Meteorological Organization, Geneva, Switzerland, \[https://globalcryospherewatch.org/reference/documents/files/GCW\\\_IP\\\_v1.7.pdf\]\(https://globalcryospherewatch.org/reference/documents/files/GCW\_IP\_v1.7.pdf\), 2016.](#)
- Kinar, N. J., and Pomeroy, J. W.: Measurement of the physical properties of the snowpack. *Rev. Geophys.* 53, 481–544. doi: 10.1002/2015RG000481, 2015.
- King J., Kelly, R., Kasurak, A., Duguay, C., Gunn, G., Rutter, N., Watts, T., and Derksen C.: Spatio-temporal influence of tundra snow properties on Ku-band (17.2 GHz) backscatter. *J. Glaciol.*, 61(226), doi: 10.3189/2015JoG14J020, 2015. **(Radar)**
- Kirkham, J.D., Koch, I., Saloranta, T.M., Litt, M., Stigter, E.E., Møen, K., Thapa, A., Melvold, K., and Immerzeel, W.W.: Near Real-Time Measurement of Snow Water Equivalent in the Nepal Himalayas. *Front. Earth Sci.* 7:177. doi: 10.3389/feart.2019.00177, 2019. **(GMON)**
- Koch, F., Henkel, P., Appel, F., Schmid, L., Bach, H., Lamm, M., Prasch, M., Jürg Schweizer, J., and Mauser, W.: Retrieval of snow water equivalent, liquid water content, and snow height of dry and wet snow by combining GPS signal

- attenuation and time delay. *Water Resour. Res.*, 55, 4465–4487. <https://doi.org/10.1029/2018WR024431>, 2019. **(GNSSr)**
- Koh, G., Yankielun, N.E., and Baptista, A.I.: Snow cover characterization using multiband FMCW radars. *Hydrol. Process.*, 10, 1609–1617, 1996. **(FMCW-Radar)**
- [Kramer, D., Langlois, A., Royer, A., Madore, J.-B., King, J., McLennan, D. and Boisvert-Vigneault, É.: Assessment of Arctic snow stratigraphy and water equivalent using a portable Frequency Modulated Continuous Wave RADAR. Submitted to Cold Regions Science and Technology, ID.: CRST-D-21-00297, \(2021\).](#)
- Laliberté, J., Langlois, A., Royer, A., Madore, J.-B., and Gauthier, F.: Retrieving high contrasted interfaces in dry snow using a frequency modulated continuous wave (FMCW) Ka-band radar: a context for dry snow stability, *Physical Geography*, In revision (TPHY-S-21-00044), 2021. **(FMCW-Radar)** **To be updated**
- Langlois, A., Royer, A. and Goïta, K.: Analysis of simulated and spaceborne passive microwave brightness temperature using in situ measurements of snow and vegetation properties. *Can J Remote Sens.* 36(S1), 135–148. doi:10.5589/m10-016, 2010.
- Langlois, A.: Applications of the PR Series Radiometers for Cryospheric and Soil Moisture Research. Publisher: Radiometrics Corporation  
[https://www.researchgate.net/publication/299372180 Applications of the PR Series Radiometers for Cryospheric and Soil Moisture Research](https://www.researchgate.net/publication/299372180_Applications_of_the_PR_Series_Radiometers_for_Cryospheric_and_Soil_Moisture_Research), 2015. **(Radiometer)**
- Larson, K. M., and Small, E. E.: Normalized microwave reflection index: A vegetation measurement derived from GPS networks, *IEEE J. Sel. Topics Appl. Earth Observ. Remote Sens.*, 7(5), 1501-1511, doi: 10.1109/JSTARS.2014.2300116, 2014. **(GNSSr)**
- Larson, K. M.: GPS interferometric reflectometry: Applications to surface soil moisture, snow depth, and vegetation water content in the western United States. *Wiley Interdisciplinary Reviews: Water*, 3(6), 775–787. <https://doi.org/10.1002/wat2.1167>, 2016. **(GNSSr)**
- Larson, K., Gutmann, E., Zavorotny, V., Braun, J., Williams, M., and Nievinski, F.: Can we measure snow depth with GPS receivers? *Geophys. Res. Lett.*, 36, L17502. <https://doi.org/10.1029/2009GL039430>, 2009. **(GNSSr)**
- Larue, F., Royer, A., De Sève, D., Roy, A., Picard, G., Vionnet, V.: Simulation and assimilation of passive microwave data using a snowpack model coupled to a calibrated radiative transfer model over North-Eastern Canada, *Water Resour. Res.*, 54, 4823–4848, <https://doi.org/10.1029/2017WR022132>, 2018.
- Leinss, S., Wiesmann, A., Lemmetyinen, J., and Hajnsek, I.: Snow Water Equivalent of Dry Snow Measured by Differential Interferometry. *IEEE J. Sel. Topics Appl. Earth Observ. Remote Sens.*, 8(8), 3773-379, 2015. **(SnowScat radar)**
- Lejeune, Y., Dumont, M., Panel, J.-M., Lafaysse, M., Lapalus, P., Le Gac, E., Lesaffre, B., and Morin, S.: 57 years (1960–2017) of snow and meteorological observations from a mid-altitude mountain site (Col de Porte, France, 1325 m of altitude), *Earth Syst. Sci. Data*, 11, 71–88, <https://doi.org/10.5194/essd-11-71-2019>, 2019.
- [López-Moreno, J.I., Leppänen, L., Luks, B., Holko, L., Picard, G., Sanmiguel-Vallelado, A., Alonso-González, E., Finger, D.C., Arslan, A.N., Gillemot, K., Sensoy, A., Sorman, A., Ertaş, M. C., Fassnacht, S.R., Fierz, C., and Marty, C.: Intercomparison of measurements of bulk snow density and water equivalent of snow cover with snow core samplers: Instrumental bias and variability induced by observers. \*Hydrol. Proc.\*, 34, 3120-3133, <https://doi.org/10.1002/hyp.13785>, 2020. \*\*\(Snow core\)\*\*](#)
- Marshall, H.-P., and Koh, G.: FMCW radars for snow research. *Cold Reg. Sci. Technol.*, 52, 118–131, 2008.
- Marshall, H.-P., Schneebeli, M., and Koh, G. Snow stratigraphy measurements with high-frequency FMCW radar: Comparison with snow micro-penetrator. *Cold Reg. Sci. Technol.*, 47, 108–117, 2007. **(FMCW-Radar)**
- Marshall, H.-P., Koh, G., and Forster, R.: Estimating alpine snowpack properties using FMCW radar. *Ann. Glaciol.*, 40, 157–162, 2005. **(FMCW-Radar)**
- [Martin, J.-P., Houdayer, A., Lebel, C., Choquette, Y., Lavigne, P., and Ducharme, P.: An unattended gamma monitor for the determination of snow water equivalent \(SWE\) using the natural ground gamma radiation. 2008 IEEE Nuclear Science Symposium and Medical Conference, P. Sellin, Ed., IEEE, 983–988, 2008. \*\*\(CRNP\)\*\*](#)
- Matzler, C.: Microwave permittivity of dry snow, *IEEE Trans. Geosci. Remote Sens.*, 34, 573–581, <https://doi.org/10.1109/36.485133>, 1996.
- Meloche, J., Langlois, A., Rutter, N., Royer, A., King, J., and Walker, B.: Characterizing Tundra snow sub-pixel variability to improve brightness temperature estimation in satellite SWE retrievals, *The Cryosphere Discussion* (Submitted to 2021-156), 2021. **To be updated**



- Meredith, M., Sommerkorn, M., Cassotta, S., Derksen, C., Ekaykin, A., Hollowed, A., Kofinas, G., Mackintosh, A., Melbourne-Thomas, J., Muelbert, M.M.C., Ottersen, G., Pritchard, H., Schuur, E.A.G.: Polar Regions. In: IPCC Special Report on the Ocean and Cryosphere in a Changing Climate [H.-O. Pörtner, D.C. Roberts, V. Masson-Delmotte, P. Zhai, M. Tignor, E. Poloczanska, K. Mintenbeck, A. Alegría, M. Nicolai, A. Okem, J. Petzold, B. Rama, N.M. Weyer (eds.)]. <https://www.ipcc.ch/srocc/chapter/chapter-3-2/>, 2019.
- Murray, R. M., and Holbert, K. E.: Nuclear Energy: An Introduction to the Concepts, Systems, and Applications of Nuclear Processes, Eighth Edition, Imprint Butterworth-Heinemann, Elsevier Inc., 624 p. <https://doi.org/10.1016/C2016-0-04041-X>, 2020. **(CRNP)**
- Okorn, R., Brunnhofer, G., Platzer, T., Heilig, A., Schmid, L., Mitterer, C., Schweizer, J., and Eisen, O.: Upward-looking L-band FMCW radar for snow cover monitoring. *Cold Reg. Sci. Technol.*, 103, 31–40, 2014. **(FMCW-Radar)**
- Paquet, E. and Laval, M.T.: Retour d'expérience et perspectives d'exploitation des Nivomètres à Rayonnement Cosmique d'EDF / Operation feedback and prospects of EDF Cosmic-Ray Snow Sensors. *La Houille Blanche* 2006-2, 113-119, 2006. **(CRNP)**
- Paquet, E., Laval, M., Basalae, L. M., Belov, A., Eroshenko, E., Kartyshev, V., Struminsky, A., and Yanke, V.: An application of cosmic-ray neutron measurements to the determination of the snow-water equivalent, *Proc. 30th Int. Cosm. Ray Conf.*, Mexico City, Mexico, 2008, 1, 761– 764, 2008. **(CRNP)**
- Peng, Z., and Li, C.: Portable Microwave Radar Systems for Short-Range Localization and Life Tracking: A Review, *Sensors*, 19, 1136, 2019. **(FMCW-Radar)**
- Peterson, N., and Brown, J.: Accuracy of snow measurements, In *Proceedings of the 43rd Annual Meeting of the Western Snow Conference*, Coronado, California, 1-5, 1975. **(Snow core)**
- Pieraccini, M., and Miccinesi, L.: Ground-Based Radar Interferometry: A Bibliographic Review, *Remote Sens.*, 11(9), 1029, 2019. <https://doi.org/10.3390/rs11091029>. **(Radar)**
- Pirazzini, R., Leppänen, L., Picard, G., López-Moreno, J. I., Marty, C., Macelloni, G., Kontu, A., von Lerber, A., Tanis, C. M., Schneebeli, M., de Rosnay, P., and Arslan, A. N.: European in-situ snow measurements: practices and purposes, *Sensors*, 18, 2016. doi: 10.3390/s18072016, 2018.
- [Pomerleau, P., Royer, A., Langlois, A., Cliche, P., Courtemanche, B., Madore, J.B., Picard, G. and Lefebvre, É.: Low Cost and Compact FMCW 24 GHz Radar Applications for Snowpack and Ice Thickness Measurements, \*Sensors\* 20, 14, 3909. https://doi.org/10.3390/s20143909](https://doi.org/10.3390/s20143909), 2020. **(FMCW-Radar)**
- Prince, M., Roy, A., Royer, A., and Langlois, A.: Timing and Spatial Variability of Fall Soil Freezing in Boreal Forest and its Effect on SMAP L-band Radiometer Measurements, *Remote Sens. Environ.*, 231, 111230, 2019.
- Proksch, M., Rutter, N., Fierz, C., and Schneebeli, M.: Intercomparison of snow density measurements: Bias, precision, and vertical resolution, *Cryosphere*, 10, 371–384, 2016.
- Rasmussen, R., Baker, B., Kochendorfer, J., Meyers, T., Landolt, S., Fischer, A. P., Black, J., Thériault, J. M., Kucera, P., Gochis, D., Smith, C., Nitu, R., Hall, M., Ikeda, K., and Gutmann, E.: How Well Are We Measuring Snow: The NOAA/FAA/NCAR Winter Precipitation Test Bed, *Bull. Am. Meteorol. Soc.*, 93, 811–829, 2012. **(Snow core)**
- Rodriguez-Morales, F., Gogineni, S., Leuschen, C.J., Paden, J.D., Li, J., Lewis, C. C., Panzer, B., Alvestegui, D. G-G., Patel, A., Byers, K., Crowe, R., Player, K., Hale, R., Arnold, E., Smith, L., Gifford, C., Braaten, D., and Panton, C.: Advanced multifrequency radar instrumentation for polar research. *IEEE Trans. Geosci. Remote Sens.* 52, 2824–2842, 2014. **(FMCW-Radar)**
- Roy, A., Royer, A., St-Jean-Rondeau, O., Montpetit, B., Picard, G., Mavrovic, A., Marchand, N., and Langlois, A.: Microwave snow emission modeling uncertainties in boreal and subarctic environments, *The Cryosphere*, 10, 623–638, <http://www.the-cryosphere.net/10/623/2016/> doi:10.5194/tc-10-623-2016, 2016. **(Radiometer)**
- Roy, A., Toose, P., Williamson, M., Rowlandson, T., Derksen, C., Royer, A., Berg, A., Lemmetyinen, J., and Arnold, L.: Response of L-Band brightness temperatures to freeze/thaw and snow dynamics in a prairie environment from ground-based radiometer measurements, *Remote Sens. Environ.*, 191, 67-80, 2017. **(Radiometer)**
- Rutter, N., Sandells, M. J., Derksen, C., King, J., Toose, P., Wake, L., Watts, T., Essery, R., Roy, A., Royer, A., Marsh, P., Larsen, C., and Sturm, M.: Effect of snow microstructure variability on Ku-band radar snow water equivalent retrievals, *The Cryosphere*, 13, 3045–3059, <https://doi.org/10.5194/tc-13-3045-2019>, 2019.
- Rutter, N., Sandells, M., Derksen, C., Toose, P., Royer, A., Montpetit, B., Lemmetyinen, J., and Pulliainen, J.: Snow stratigraphic heterogeneity within ground-based passive microwave radiometer footprints: implications for emission modeling, *J. Geophys. Res. Earth Surf.*, 199, 550–565, <https://doi.org/10.1002/2013JF003017>, 2014.

- Schattan, P., Baroni, G., Oswald, S. E., Schöber, J., Fey, C., Kormann, C., Huttenlau, M., and Achleitner, S.: Continuous monitoring of snowpack dynamics in alpine terrain by aboveground neutron sensing, *Water Resour. Res.*, 53, 3615–3634, doi: 10.1002/2016WR020234, 2017. **(CRNP)**
- Schneider, M.: Automotive radar—Status and trends. In *Proceedings of the German Microwave Conference*, Ulm, Germany, 5–7 April 2005; pp. 144–147, 2005. **(FMCW-Radar)**
- Shah, R., Xiaolan Xu, Yueh, S., Sik Chae, C., Elder, K., Starr, B., and Kim, Y.: Remote Sensing of Snow Water Equivalent Using P-Band Coherent Reflection, *IEEE Geosci. Remote Sens. Lett.*, 14, 3, 309–313, doi: 10.1109/LGRS.2016.2636664, 2017. **(GNSSr)**
- Sigouin, M. J. P., and Si, B. C.: Calibration of a non-invasive cosmic-ray probe for wide area snow water equivalent measurement. *Cryosphere*, 10, 1181–1190, 2016 [www.the-cryosphere.net/10/1181/2016/](http://www.the-cryosphere.net/10/1181/2016/), 2016. **(CRNP)**
- Smith, C. D., Kontu, A., Laffin, R., and Pomeroy, J. W.: An assessment of two automated snow water equivalent instruments during the WMO solid precipitation intercomparison experiment, *Cryosphere*, 11, 101–116. doi: 10.5194/tc-11-101-2017, 2017. **(GMON)**
- [Steiner, L., Meindl, M., Fierz, C., and Geiger, A.: An assessment of sub-snow GPS for quantification of snow water equivalent, \*The Cryosphere\*, 12, 3161–3175, https://doi.org/10.5194/tc-12-3161-2018, 2018. \(GNSSr\)](https://doi.org/10.5194/tc-12-3161-2018)
- [Steiner, L., Meindl, M., and Geiger, A.: Characteristics and limitations of GPS L1 observations from submerged antennas, \*J. Geodesy\*, 93, 267–280, https://doi.org/10.1007/s00190-018-1147-x, 2019. \(GNSSr\)](https://doi.org/10.1007/s00190-018-1147-x)
- Stranden, H. B., Ree, B. L., and Møen, K. M.: Recommendations for Automatic Measurements of Snow Water Equivalent in NVE. Report of the Norwegian Water Resources and Energy Directorate, Majorstua, Oslo, Norway, 34 p., 2015. **(GMON)**
- Stuefer, S., Kane, L. D., and Liston, G. E.: In situ snow water equivalent observations in the US Arctic, *Hydrol. Res.*, 44, 21–34, <https://doi.org/10.2166/nh.2012.177>, 2013. **(Snow core)**
- Sturm, M., Taras, B., Liston, G., Derksen, C., Jones, T., and Lea J.: Estimating snow water equivalent using snow depth data and climate classes. *Journal of Hydrometeorology*, 11, 1380–1394, 2010. **(Snow core)**
- Tiuri, M., Sihvola, A., Nyfors, E., and Hallikainen, M.: The complex dielectric constant of snow at microwave frequencies. *IEEE J. Ocean. Eng.*, 9, 377–382, 1984.
- Turcan, J., and Loijens, J.: Accuracy of snow survey data and errors in snow sampler measurements, *Proc. 32nd East. Snow. Conf.*, 2-11, 1975. **(Snow core)**
- [Vather, T., Everson, C. S., and Franz, T. E.: The applicability of the cosmic ray neutron sensor to simultaneously monitor soil water content and biomass in an Acacia mearnsii Forest. \*Hydrology\*, 7\(3\), 48. https://doi.org/10.3390/hydrology7030048, 2020. \(CRNP\)](https://doi.org/10.3390/hydrology7030048)
- Vriend, N.M., McElwaine, J.N., Sovilla, B., Keylock, C.J., Ash, M., and Brennan, P. V.: High-resolution radar measurements of snow avalanches, *Geophys. Res. Lett.*, 40, 727–731, 2013. **(FMCW-Radar)**
- [Wallbank, J.R., Cole, S.J., Moore, R.J., Anderson, S.R., Mellor, E.J.: Estimating snow water equivalent using cosmic-ray neutron sensors from the COSMOS-UK network. \*Hydrological Processes\*, 35:e14048. https://doi.org/10.1002/hyp.14048, 2021. \(CRNP\)](https://doi.org/10.1002/hyp.14048)
- Werner, C., Suess, M., Wegmüller, U., Frey, O., and Wiesmann A.: The Esa Wideband Microwave Scatterometer (Wbscat): Design and Implementation, in *Proc. IGARSS 2019 - IEEE International Geoscience and Remote Sensing Symposium*, 8339–8342, doi: 10.1109/IGARSS.2019.8900459, 2019. **(SnowScat)**
- Werner, C., Wiesmann, A., Strozzi, T., Schneebeli, M., and Mätzler, C.: The SnowScat ground-based polarimetric scatterometer: Calibration and initial measurements from Davos Switzerland, in *Proc. IEEE Int. Geosci. Remote Sens. Symp. (IGARSS'10)*, Jul. 2010, 2363–2366, 2010. **(SnowScat)**
- Wiesmann, A., Werner, C., Strozzi, T., Matzler, C., Nagler, T., Rott, H., Schneebeli, M., and Wegmüller, U.: SnowScat, X- to Ku-Band Scatterometer Development, in *Proc. of ESA Living Planet Symposium*, Bergen 28.6. - 2.7. [https://gamma-rs.ch/uploads/media/Instruments\\_Info/gamma\\_snowscat.pdf](https://gamma-rs.ch/uploads/media/Instruments_Info/gamma_snowscat.pdf), 2010. **(SnowScat)**
- Wiesmann, A., Werner, C., Wegmüller, U., Schwank, M., and Matzler, C.: ELBARA II, L-band Radiometer for SMOS Cal/Val Purposes, [https://gamma-rs.ch/uploads/media/Instruments\\_Info/ELBARAII\\_poster.pdf](https://gamma-rs.ch/uploads/media/Instruments_Info/ELBARAII_poster.pdf), 2021. **(Radiometer)**
- Wigneron, J.P., Jackson, T.J., O'Neill, P., De Lannoy, G.J., de Rosnay, P., Walker, J.P., Ferrazzoli, P., Mironov, V., Bircher, S., Grant, J.P., Kurum, M., Schwank, M., Munoz-Sabater, J., Das, N., Royer, A., Al-Yaari, A., Bitar, A. Fernandez-Moran, R., Lawrence, H., Mialon, A., Parrons, M., Richaume, P., Delwart, S., and Kerr Y.: Modelling the passive microwave signature from land surfaces: A review of recent results and application to the L-Band SMOS & SMAP soil moisture retrieval algorithms, *Remote Sens. Environ.*, 192, 238–262, 2017. **(Radiometer)**

- Work, R. A., Stockwell, H. J., Freeman, T. G., and Beaumont, R. T.: Accuracy of field snow surveys, western United States, including Alaska, Cold Regions Research and Engineering Laboratory (U.S.) Technical report, 163, 49 p., <https://hdl.handle.net/11681/5580>. 1965. **(Snow core)**
- Wright, M., Kavanaugh, K., and Labine C.: Performance Analysis of the GMON3 Snow Water Equivalency Sensor. Proceedings of The Western Snow Conference. Stateline, NV, USA, April 2011. Poster on line, <https://www.campbellsci.ca/cs725>, 2011 **(GMON)**
- Wright, M.: CS725 Frozen Potential: The Ability to Predict Snow Water Equivalent is Essential. METEOROLOGICAL TEChnOLOGy InTERnATIOnAL, August 2013, 122-123, <https://www.meteorologicaltechnologyinternational.com>, 2013. **(GMON)**
- Xu, X., Baldi, C., Bleser, J.-W., Lei, Y., Yueh, S., and Esteban-Fernandez, D.: Multi-Frequency Tomography Radar Observations of Snow Stratigraphy at Fraser During SnowEx, in Proceedings of the IGARSS 2018-2018 IEEE International Geoscience and Remote Sensing Symposium, Valencia, Spain, 22–27 July 2018, 2018. **(FMCW-Radar)**
- Yankielun, N., Rosenthal, W., and Robert, D.: Alpine snow depth measurements from aerial FMCW radar. Cold Reg. Sci. Technol., 40, 123–134, 2004. **(FMCW-Radar)**
- Yankielun, N.E., Ferrick, M.G., and Weyrick, P. B.: Development of an airborne millimeter-wave FM-CW radar for mapping river ice, Can. J. Civ. Eng., 20, 1057–1064, 1993. **(FMCW-Radar)**
- Yao, H., Field, T., McConnell, C., Beaton, A., and James A.L.: Comparison of five snow water equivalent estimation methods across categories. Hydrol. Process., 32, 1894–1908, <https://doi.org/10.1002/hyp.13129>, 2018. **(GMON)**